Intranasal Vaccination with a Lentiviral Vector Strongly Protects against SARS-CoV-2 in Mouse and Golden Hamster Preclinical Models

Min-Wen Ku[1£], Maryline Bourgine[1,2£], Pierre Authié[1£], Jodie Lopez[1], Kirill Nemirov[1], Fanny Moncoq[1], Amandine Noirat[1], Benjamin Vesin[1], Fabien Nevo[1], Catherine Blanc[1], Philippe Souque[2], Houda Tabbal[3], Emeline Simon[3,4], Marine Le Dudal[5], Françoise Guinet[6], Laurence Fiette[5], Hugo Mouquet[7], François Anna[1], Annette Martin[3], Nicolas Escriou[8], Laleh Majlessi[1,$,#,*] and Pierre Charneau[1,2,$*]

[1]Institut Pasteur-TheraVectys Joint Lab, Virology Department, 28 rue du Dr. Roux, Paris F-75015, France

[2]Molecular Virology and Vaccinology Unit, Virology Department, Institut Pasteur

[3]Molecular Genetics of RNA Viruses Unit, Virology Department, Institut Pasteur, CNRS UMR3569, Université de Paris, Paris-F 75015, France

[4]Université de Paris, Paris F-75006, France

[5]IMMR, 42 boulevard Jourdan, Paris F-75014, France

[6]Lymphocytes and Immunity Unit, Immunology Department, Institut Pasteur

[7]Laboratory of Humoral Immunology, Immunology Department, Institut Pasteur, INSERM U1222

[8]Innovation Lab, Vaccines, Institut Pasteur

[£]These authors contributed equally

[$]Senior authors

[#]Lead Contact

[*]Corresponding authors: (laleh.majlessi@pasteur.fr, pierre.charneau@pasteur.fr)

Summary

To develop a vaccine candidate against COVID-19, we generated a Lentiviral Vector (LV), eliciting neutralizing antibodies against the Spike glycoprotein of SARS-CoV-2. Systemic vaccination by this vector in mice, in which the expression of the SARS-CoV-2 receptor hACE2 has been induced by transduction of respiratory tract cells by an adenoviral vector, conferred only partial protection, despite an intense serum neutralizing activity. However, targeting the immune response to the respiratory tract through an intranasal boost with this LV resulted in > 3 log10 decrease in the lung viral loads and avoided local inflammation. Moreover, both integrative and non-integrative LV platforms displayed a strong vaccine efficacy and inhibited lung deleterious injury in golden hamsters, which are naturally permissive to SARS-CoV-2 replication and restitute the human COVID-19 physiopathology. Our results provide evidence of marked prophylactic effects of the LV-based vaccination against SARS-CoV-2 and designate the intranasal immunization as a powerful approach against COVID-19.

Keywords

Lentiviral vectors, intranasal vaccination, mucosal immunity, boost-target, immunoglobulin A, lung inflammation, beta-coronavirus, in vivo Ad5 transduction, respiratory tracts, golden hamsters, neutralizing antibodies.

Highlights

A lentiviral vector encoding for Spike predicts a promising COVID-19 vaccine

Targeting the immune response to the upper respiratory tract is key to protection

Intranasal vaccination induces protective mucosal immunity against SARS-CoV-2

Lung anti-Spike IgA responses correlate with protection and reduced inflammation

50 **Introduction**

51 The new Severe Acute Respiratory Syndrome beta-coronavirus 2 (SARS-CoV-2) that emerged in
52 late 2019 in Wuhan, China, is extraordinarily contagious and fast-spreading across the world (Guo et
53 al., 2020). Compared to the previously emerged SARS or Middle East Respiratory Syndrome (MERS)
54 coronaviruses, SARS-CoV-2 causes unprecedented threat on global health and tremendous socio-
55 economic consequences. Therefore, the development of effective prophylactic vaccines against SARS-
56 CoV-2 is an absolute imperative to contain the spread of the epidemic and to prevent the development
57 of CoronaVirus Disease 2019 (COVID-19)-associated symptoms such as deleterious inflammation and
58 progressive respiratory failure (Amanat and Krammer, 2020).

59 Coronaviruses are enveloped, non-segmented positive-stranded RNA viruses, characterized by their
60 envelope-anchored Spike (S) glycoprotein (Walls et al., 2020). The SARS-CoV-2 S (S_{CoV-2}) is a
61 $(180\ kDa)_3$ homotrimeric class I viral fusion protein, that engages the carboxypeptidase Angiotensin-
62 Converting Enzyme 2 (ACE2) expressed on host cells. The monomer of S_{CoV-2} protein possesses an
63 ectodomain, a transmembrane anchor domain, and a short internal tail. S_{CoV-2} is activated by a two-step
64 sequential proteolytic cleavage to initiate fusion with the host cell membrane. Subsequent to S_{CoV-2}-
65 ACE2 interaction, through a conformational reorganization, the extracellular domain of S_{CoV-2} is first
66 cleaved at the highly specific furin $682^{RRAR}685$ site (Guo et al., 2020; Walls et al., 2020), a key factor
67 determining the pathological features of the virus, linked to the furin ubiquitous expression (Wang et
68 al., 2020). The resulting subunits are: (i) S1, which harbors the ACE2 Receptor Binding Domain
69 (RBD), with the atomic contacts restricted to the ACE2 protease domain, and (ii) S2, which bears the
70 membrane-fusion elements. Similar to S_{CoV-1}, the shedding of S1 renders accessible on S2 the second
71 proteolytic cleavage site 797^{R}, namely S2' (Belouzard et al., 2009). Depending on the cell or tissue
72 type, one or several host proteases, including furin, trypsin, cathepsins or transmembrane protease
73 serine protease-2 or -4, can be involved in this second cleavage step (Coutard et al., 2020). The
74 consequent "fusogenic" conformational changes of S result in the exposure of a Fusion Peptide (FP),
75 adjacent to S2'. Insertion of FP to the host cell/vesicle membrane primes the fusion reaction, which in
76 turn leads to the viral RNA release into the host cytosol (Lai et al., 2017). The facts that the S_{CoV-2}-
77 ACE2 interaction is the only mechanism thus far identified for the host cell infection by SARS-CoV-
78 2, and that the RBD contains numerous conformational B-cell epitopes (Walls et al., 2020), designate
79 this viral envelope glycoprotein as the main target for neutralizing antibodies (NAbs).

80 Compared to: (i) attenuated or inactivated viral vaccine candidates which require extensive safety
81 testing, (ii) nucleic acid with moderate immunogenicity in human linked to the difficulty of their
82 delivery to targeted immune cells (Hobernik and Bros, 2018), (iii) protein vaccines which require the
83 use of adjuvants and boosting, viral vector vaccines such as adenoviral vectors are interesting vaccine
84 candidates that generate strong immune responses. However, adenoviral vectors are target of pre-
85 existing immunity in the human population, which largely reduces their immunogenicity (Rosenberg

86 et al., 1998; Schirmbeck et al., 2008). Non-replicative lentiviral vaccinal vectors (LV) possess a large
87 potential at eliciting strong and long-lasting adaptive immunity, including Ab responses (Di Nunzio et
88 al., 2012; Hu et al., 2011; Ku et al., 2020; Zennou et al., 2000). These vectors induce very minor
89 inflammation (Lopez et al., in preparation) and their safety has been demonstrated in human in a phase
90 1 HIV-1 vaccine trial (2011-006260-52 EN). In addition, LV are pseudo-typed with the envelope
91 glycoprotein of Vesicular Stomatitis Virus (VSV-G), to which human population is barely exposed.
92 This minimizes the risk of vaccine efficacy reduction linked to a pre-existing cross-reactive immunity
93 (Hu et al., 2011).
94 To develop a vaccine candidate able to induce NAbs specific to S_{CoV-2}, we generated LV coding for:
95 (i) S1 alone (LV::S1), (ii) S1-S2 ectodomain, without the transmembrane and internal tail domains
96 (LV::S1-S2), or (iii) full-length, membrane anchored form of S (LV::S_{FL}). We established that LV::S_{FL}
97 gave rise to elevated amounts of NAbs, which inhibit $ACE2^+$ host-cell invasion by S_{CoV-2}-pseudo-typed
98 virions. Anti-S_{CoV-2} $CD8^+$ T cell effectors were also efficiently induced in LV::S_{FL}-immunized mice.
99 Moreover, in a mouse model in which the expression of human ACE2 (hACE2) was induced in the
100 respiratory tracts by instillation with an adenoviral vector serotype 5 (Ad5), as well as in SARS-CoV-
101 2-susceptible golden hamsters, we demonstrated a strong prophylactic effect of LV::S_{FL} immunization
102 against the replication of a SARS-CoV-2 clinical isolate, accompanied by the reduction of infection-
103 related inflammation in the lungs. Importantly, boost/target immunization with LV::S_{FL} via nasal route
104 was instrumental in the protection efficacy. Our virological, immunological and histopathological
105 criteria in two preclinical animal models provided the proof-of-principle evidence of marked
106 prophylactic effects of LV-based vaccine strategies against SARS-CoV-2, and requirement for mucosal
107 immunization to reach vigorous protective lung immunity against COVID-19.

Results

Induction of antibody responses by LV encoding SARS-CoV-2 Spike protein variants

To develop a vaccine candidate able to induce NAbs against S_{CoV-2}, we generated LV harboring, under the transcriptional control of the cytomegalovirus (CMV) immediate-early promoter, codon-optimized sequences encoding for: (i) S1 alone (LV::S1), (ii) S1-S2 ectodomain, without the transmembrane and C-terminal short internal tail (LV::S1-S2), and (iii) full-length, membrane anchored form of S (LV::S_{FL}), which all harbor the RBD (Figure 1A, Figure S1), albeit with potential conformational heterogeneities (Yuan et al., 2020). To evaluate the humoral responses induced by these vectors, C57BL/6 mice (n = 4/group) were immunized by a single intraperitoneal (i.p.) injection of 1 × 10^7 Transduction Units (TU) of either LV, or an LV encoding GFP as negative control. Anti-S_{CoV-2} Ab responses were investigated in the sera at weeks 1, 2, 3, 4 and 6 post immunization (Figure 1B). In LV::S_{FL} or LV::S1-S2-immunized mice, anti-S_{CoV-2} immunoglobulin G (IgG) were detectable as early as 1 week post immunization and increased progressively until week 6 post immunization, achieving mean titer (1/dilution) ± SEM of (4.5 ± 2.9) × 10^6 or (1.5 ± 1) × 10^6, respectively. In comparison, anti-S_{CoV-2} IgG titers were 2 orders of magnitude lower, i.e., (7.1 ± 6.1) ×10^4, in their LV::S1-immunized counterparts.

Sera were then evaluated for their capacity to neutralize SARS-CoV-2, using a reliable neutralization assay based on NAb-mediated inhibition of hACE2$^+$ cell invasion by non-replicative LV particle surrogates, pseudo-typed with S_{CoV-2} (Sterlin et al., 2020). Such S_{CoV-2} pseudo-typed LV particles, harbor a luciferase reporter gene, which allows quantitation of the hACE2$^+$ host cell invasion. In this assay, the luciferase activity is inversely proportional to the neutralization efficiency of NAbs present in biological fluids. Fine comparison, by 50% Effective Concentrations (EC50) assays of the sera from the LV::S1-, LV::S1-S2- or LV::S_{FL}-immunized mice clearly established that LV::S_{FL} was the most potent vector at inducing anti-S_{CoV-2} NAbs (Figure 1C). Moreover, neutralization activities were correlated with anti-S_{CoV-2} IgG titers only in the sera of LV::S_{FL}-immunized mice (Figure 1D). These results suggest that in the S1-S2 or S1 polypeptides, the conformations of relevant B-cell epitopes are distinct from those of the native S_{FL} and that the blocking action of NAbs is linked to their specific recognition of the native conformational epitopes. Comparison of the sera from the LV::S_{FL}-immunized mice and a cohort of mildly symptomatic infected individuals living in Crépy-en-Valois, one of the first epidemic zones to appear in France, revealed similar mean neutralizing activities (Figure 1E). These data predict a potentially protective humoral response induced by LV::S_{FL}.

LV::S_{FL}-immunized C57BL/6 mice (n = 3) also displayed strong anti-S_{CoV-2} T-cell responses, as detected at week 2 post immunization by IFNγ ELISPOT-based epitope mapping, applied to splenocytes stimulated with distinct pools of 15-mer peptides spanning the full-length S_{CoV-2} (Figure 2A). Significant amounts of responding T cells were detected for 6 out of 16 peptide pools.

143 Deconvolution of these positive pools allowed identification of S:256-275
144 (SGWTAGAAAYYVGYLQPRTF), S:536-550 (NKCVNFNFNGLTGTG) and S:576:590
145 (VRDPQTLEILDITPC) immunodominant epitopes, giving rise to > 2000 Spot Forming Unit (SFU) /
146 spleen (Figure 2B). These epitopes elicited $CD8^+$ - but not $CD4^+$ - T cells, as assessed by intracellular
147 cytokine staining (Figure 2C). The predominant $CD8^+$ phenotype of these T cells is in accordance with
148 the favored orientation of LV-encoded antigens to the MHC-I presentation pathway (Hu et al., 2011).
149 We also identified S:441-455 (LDSKVGGNYNYLYRL), S:671-685 (CASYQTQTNSPRRAR) and
150 S:991-1005 (VQIDRLITGRLQSLQ) subdominant epitopes, which gave rise to < 2000 SFU / spleen
151 in ELISPOT assay (Figure 2B).

152 **Establishment of a murine model expressing hACE2 in the respiratory tracts**

153 As S_{CoV-2} does not interact well with murine ACE2, wild-type laboratory mice are not permissive to
154 replication of SARS-CoV-2 clinical isolates. Therefore, we sought to develop a murine model in which
155 human ACE2 (hACE2) expression was induced in the respiratory tracts and pulmonary mucosa to
156 evaluate the LV::S_{FL} vaccine efficacy. This method has been successfully used to establish the
157 expression of human DPP4 for the study of mouse infection with MERS-CoV (Zhao et al., 2014) and
158 also for hACE2 during the preparation of this manuscript (Sun et al., 2020). We generated an Ad5
159 vector to deliver the gene encoding for hACE2 under the transcriptional control of the CMV promoter
160 (Ad5::hACE2) in an episomal form. We first checked in vitro the potential of the Ad5::hACE2 vector
161 to transduce HEK293T cells by Reverse Transcriptase (RT)-PCR (Figure 3A). To achieve in vivo
162 transduction of respiratory tract cells, we instilled intranasally (i.n.) 2.5×10^9 Infectious Genome Units
163 (IGU) of Ad5::hACE2 into C57BL/6 mice. Four days later, the hACE2 protein expression was
164 detectable in the lung cell homogenate by Western Blot (Figure 3B). To get more insights into the in
165 vivo expression profile of a transgene administered under these conditions, we instilled i.n. the same
166 dose of an Ad5::GFP reporter vector into C57BL/6 mice. As evaluated by flow cytometry, 4 days post
167 instillation, the GFP reporter was expressed not only in the lung epithelial $EpCam^+$ cells, but also in
168 lung immune cells, as tracked by the CD45 pan-hematopoietic marker (Figure 3C), showing that
169 through this approach the transduction was efficiently achieved in epithelial cells, although not
170 restricted to these cells.

171 To evaluate the permissibility of such hACE2-transduced mice to SARS-CoV-2 infection, 4 days
172 after i.n. pretreatment with either Ad5::hACE2 or an empty Ad5 control vector, C57BL/6 mice were
173 inoculated i.n. with 1×10^5 $TCID_{50}$ (Median Tissue Culture Infectious Dose) of a SARS-CoV-2 clinical
174 isolate (BetaCoV/France/IDF0372/2020), which was isolated in January 2020 from a COVID-19
175 patient by the National Reference Centre for Respiratory Viruses (Institut Pasteur, Paris, France)
176 (Lescure et al., 2020). The lung viral loads, determined at 2 days post inoculation (dpi) by reverse
177 transcription and quantitative real-time PCR (qRT-PCR), were as high as $(4.4 \pm 1.8) \times 10^9$ copies of

178 SARS-CoV-2 RNA in Ad5::hACE2-pretreated mice, compared to only (6.2 ± 0.5) × 10^5 copies in
179 empty Ad5-pretreated mice, or (4.0 ± 2.9) × 10^5 copies in un-pretreated mice (Figure 3D). In the latter
180 two control groups, these copy numbers corresponded to the input viral RNA, as determined in
181 Ad5::hACE2-pretreated mice, inoculated with equivalent amounts of heat-killed viral particles (Figure
182 3D). At 4 dpi, the lung viral loads were maintained in Ad5::hACE2-pretreated mice (2.8 ± 1.3 × 10^9
183 copies), whereas a drop to (1.7 ± 2.3) × 10^4 or (3.9 ± 5.1) × 10^3 copies was observed in empty Ad5-
184 pretreated or non-pretreated mice, respectively. In Ad5::hACE2-pretreated mice, the viral loads were
185 still detectable at 7 dpi ((1.33 ± 0.9) × 10^6 copies).

186 Ad5::hACE-2 i.n. instillation induced $CD45^+$ cell recruitment to the lungs (Figure 3E). However,
187 no pro-inflammatory effect was seen with a lower dose of 4 x 10^8 IGU/mouse (Figure 3E), which still
188 conferred full permissibility to SARS-CoV-2 replication (Figure 3F), and this dose was therefore
189 chosen for the subsequent experiments described below. In this model of permissive mice, SARS-CoV-
190 2 infection resulted in widespread infiltration of the lung interstitium by mononuclear inflammatory
191 cells, i.e., lymphocytes and macrophages, at 3 dpi (Figure S2).

192 These results show that pretreatment of mice with appropriate doses of Ad5::hACE2 can render
193 mice permissive to SARS-CoV-2 replication without inducing Ad5-mediated inflammation, thus
194 providing a valuable model for vaccine or drug studies.

195 **Intranasal boost with LV::S_{FL} protects strongly against SARS-CoV-2 in mice**

196 To investigate the prophylactic potential of LV::S_{FL} against SARS-CoV-2, C57BL/6 mice (*n* = 4-
197 5/group) were injected i.p. with a single dose of 1 × 10^7 TU of LV::S_{FL} or a negative control LV (sham).
198 At week 7 post immunization, mice were pretreated with Ad5::hACE2, and 4 days later, inoculated i.n.
199 with 1 × 10^5 $TCID_{50}$ of SARS-CoV-2 (Figure S3A). At 3 dpi, the lung viral loads in LV::S_{FL}-vaccinated
200 mice were reduced by ~ 6.5 folds, i.e., mean ± SD of (5.5 ± 3.8) × 10^8 SARS-CoV-2 RNA copies
201 compared to (3.1 ± 1.9) × 10^9 or (4.3 ± 3.0) × 10^9 copies in the un- or sham-vaccinated mice,
202 respectively (Figure S3B). Therefore, a single i.p. LV::S_{FL} injection provided partial protection in the
203 lung, despite intense serum NAb activity.

204 To further improve the prophylactic effect, we evaluated the prime-boost or prime-target
205 approaches. C57BL/6 mice (*n* = 4-5/group) were primed i.p. with 1 × 10^7 TU of LV::S_{FL} or a control
206 LV at week 0, and then boosted at week 3 with: (i) 1 × 10^7 TU of the same LV via the i.p. route
207 ("LV::S_{FL} i.p.-i.p.", prime-boost), or (ii) with 3 × 10^7 TU via the i.n. route ("LV::S_{FL} i.p.-i.n.", prime-
208 target) to attract the mediators of systemic immunity to the lung mucosa (Figure 4A). Systemic
209 boosting with LV::S_{FL} via i.p. resulted in a significant increase in the anti-S_{CoV-2} IgG titers, which was
210 more obvious when the binding was evaluated against the foldon-trimerized full-length S (Figure 4B,
211 left) than against the S1 or RBD fragments (Figure S4A). This observation may suggest that the
212 concerned B-cell epitopes are of conformational type. In contrast, mucosal targeting with LV::S_{FL} via

213 i.n. did not lead to a statistically significant improvement of anti-S_{CoV-2} IgG titers at the systemic level
214 (Figure 4B left, Figure S4A). In terms of serum neutralization potential, even though a trend to increase
215 was observed after i.p. or i.n. boost, the differences did not reach statistical significance (Figure 4B
216 right).

217 All mice were then pretreated with Ad5::hACE2 and challenged i.n. with 0.3×10^5 $TCID_{50}$ of
218 SARS-CoV-2 at week 4 post prime. At 3 dpi, the lung viral loads were significantly lower in LV::S_{FL}
219 i.p.-i.p. immunized mice, i.e., mean ± SD $(2.3 \pm 3.2) \times 10^8$, than in sham-vaccinated mice (13.7 ± 7.5)
220 $\times 10^8$ copies of SARS-CoV-2 RNA, (Figure 4C). This viral load reduction was similar to that obtained
221 with a single LV::S_{FL} administration (Figure S3B). Most importantly, after i.n. LV::S_{FL} target
222 immunization, > 3 log10 decrease in viral loads was observed and 2 out of 5 mice harbored undetectable
223 lung viral loads as determined by qRT-PCR assay. Anti-S_{CoV-2} IgG were detected in the clarified lung
224 homogenates of the partially (LV::S_{FL} i.p.-i.p.) or the fully (LV::S_{FL} i.p.-i.n.) protected mice. In contrast
225 anti-S_{CoV-2} IgA were only detectable in the fully protected LV::S_{FL} i.p.-i.n. mice (Figure 4D). Higher
226 neutralizing activity was detected in the clarified lung homogenates of LV::S_{FL} i.p.-i.n. mice than of
227 their LV::S_{FL} i.p.-i.p. counterparts (Figure 4E). Therefore, increasing the titers of NAb of IgG isotype
228 at the systemic levels did not improve the protection against SARS-CoV-2. However, a mucosal i.n.
229 target immunization, with the potential to attract immune effectors to the infection site and able to
230 induce local IgA Abs, correlated with the inhibition of SARS-CoV-2 replication.

231 Because of the importance of innate immune hyperactivity in the pathophysiology of COVID-19
232 (Vabret et al., 2020), we investigated the lung innate immune cell subsets in the non-infected controls,
233 sham-vaccinated or LV::S_{FL}-vaccinated mice inoculated with SARS-CoV-2 (Figure 5A). At 3 dpi, we
234 detected no difference in the proportions of basophils or NK cells versus total lung $CD45^+$ cells among
235 the experimental groups (Figure 5B). In sharp contrast, we detected higher proportions of alveolar
236 macrophages, dendritic cells, mast cells, $Ly6C^+$ or $Ly6C^-$ monocytes/macrophages or neutrophils
237 versus total lung $CD45^+$ cells, in sham-vaccinated mice. These observations demonstrate that in this
238 mouse model, lung SARS-CoV-2 loads correlate with the expansion of several inflammation-related
239 innate immune cell subsets, while vaccine-mediated protection dampens or prevents the inflammatory
240 reaction.

241 This was corroborated by the reduced inflammatory cytokine and chemokine contents in the RNA
242 extracted from total lung homogenates of mice immunized with "LV::S_{FL} i.p.-i.n." (Figure 5C, Figure
243 S5A) or "LV::S_{FL} i.p.-i.p." (Figure S5B) and protected against SARS-CoV-2. Significant reductions
244 were notably detected in the IL-1β, IL-6, CCL2, CCL3 and CXCL5 contents in the lungs of "LV::S_{FL}
245 i.p.-i.n."- versus sham i.p.-i.n.-vaccinated and challenged mice (Figure 5C, Figure S5A). Significant
246 reductions of TNF-α, TGF-β, IL-1β, IL-12p40, IL-17A, IL-33, CCL2, CCL3, CCL5, CXCL9 and
247 CXCL10 contents were also observed in the lungs of "LV::S_{FL} i.p.-i.p."- versus sham i.p.-i.p.-

248 vaccinated and challenged mice (Figure S5B). The expression of the other mediators tested was not
249 significantly changed (Figure S5A, C). Therefore, the conferred protection also avoided pulmonary
250 inflammation mediated by SARS-CoV-2 infection, as demonstrated by cytometric or qRT-PCR
251 approaches.

252 **Intranasal vaccination with LV::S_{FL} strongly protects against SARS-CoV-2 in golden**
253 **hamsters**

254 Outbred *Mesocricetus auratus*, so-called golden hamsters, provide a suitable pre-clinical model to
255 study the COVID-19 pathology, since the ACE2 ortholog of this species interacts productively with
256 S_{CoV-2}, supporting host cell invasion and viral replication (Sia et al., 2020). We thus investigated in this
257 model the protective effect against SARS-CoV-2 infection of vaccination by LV::S_{FL} and by an
258 integrase deficient, non-integrative version of this vector (NILV), with the prospect of application in
259 future clinical trials.

260 To assess the prophylactic effect of vaccination following prime-boost/target regimen, *M. auratus*
261 hamsters (n = 6/group) were: (i) primed i.p. with 1×10^6 TU of LV::S_{FL} and boosted i.n. at week 5 with
262 4×10^7 TU of LV::S_{FL}, ("int LV::S_{FL} i.p.-i.n. Low"), (ii) primed i.p. with 1×10^7 TU of LV::S_{FL} and
263 boosted i.n. at week 5 with 4×10^7 TU of LV::S_{FL} ("int LV::S_{FL} i.p.-i.n. High"), or (iii) primed
264 intramuscularly (i.m.) with 1×10^8 TU of NILV::S_{FL} and boosted i.n. at week 5 with 1×10^8 TU of
265 NILV::S_{FL} ("NILV::S_{FL} i.m.-i.n.") (Figure 6A). Sham-vaccinated controls received the same amounts
266 of an empty LV via i.p. and then i.n. routes. Strong and comparable anti-S_{CoV-2} IgG Abs were detected
267 by ELISA in the sera of hamsters from the three vaccinated groups, before and after the i.n. boost
268 (Figure 6B). Post boost/target serology detected neutralization activity in all groups, with the highest
269 EC50 average observed in "int LV::S_{FL} i.p.-i.n. High" individuals. Such levels were comparable to
270 those detected in COVID-19 cases or healthy contacts in humans (Figure 6C). All hamsters were
271 challenged i.n. with 0.3×10^5 $TCID_{50}$ of SARS-CoV-2 at week 5. Up to 16% weight loss was
272 progressively reached at 4 dpi in sham-vaccinated individuals, compared to a non-significant loss in
273 the LV::S_{FL}-vaccinated groups (Figure 6D). As assessed by qRT-PCR, at 2 dpi, decreases of ~ 1.2-to-
274 2 log10 were observed in the lung viral loads of "int LV::S_{FL} i.p.-i.n. Low", "int LV::S_{FL} i.p.-i.n. High"
275 and "NILV::S_{FL} i.m.-i.n." groups, compared to sham-vaccinated hamsters (Figure 6E). At 4 dpi, the
276 magnitude of viral load reductions in the vaccinated groups were much more important and reached
277 >3 log10, compared to the sham-vaccinated individuals. Using the Plaque Forming Unit (PFU) assay,
278 at 2 and 4 dpi, we detected (6.56 ± 1.88) and $(2.94 \pm 3.16) \times 10^6$ PFU/lung of sham-vaccinated controls.
279 At 2 dpi, the decrease in the viral loads were largely statistically significant in all of the LV::S_{FL}-
280 vaccinated hamsters and at 4 dpi, with the exception of one "NILV::S_{FL} i.m.-i.n." hamster, no
281 vaccinated individuals possessed detectable infectious viral particles (Figure 6F).

282 As evaluated by qRT-PCR in the total lung homogenates of the protected "int LV::S_{FL} i.p.-i.n. Low",
283 "int LV::S_{FL} i.p.-i.n. High" and "NILV::S_{FL} i.m.-i.n." groups, substantial decreases were observed at 4
284 dpi in the expression of inflammatory IFN-γ and IL-6 cytokines, anti-inflammatory IL-10 cytokine,
285 and CCL2, CCL3 and CXCL10 chemokines, compared to their unprotected sham-vaccinated
286 counterparts (Figure 7A). The other inflammatory mediators tested were not significantly modified
287 (Figure S6).

288 In sham-vaccinated and challenged hamsters, overall marked multifocal degenerative changes of
289 the bronchial/bronchiolar epithelium, moderate effacement of the epithelium, associated with mild to
290 moderate mixed inflammation in the airway lumen, and minimal multifocal interstitial mononuclear
291 cell inflammation at both time-points (Figure 7B). At 4 dpi, effacement of the respiratory epithelium
292 and mixed inflammation in the alveoli were more severe; moderate fibrin deposits were also noted. In
293 vaccinated hamsters, regardless of the regardless of the vaccine dose, lung lesions were clearly of lower
294 incidence and severity (Figure 7C). In these animals, only minimal to mild degenerative lesions and
295 minimal effacement of the bronchial/bronchiolar epithelium and occasionally mixed inflammation in
296 the airway lumen of alveoli and mononuclear infiltrates in the interstitium were observed. These
297 microscopic findings were similar after vaccination with the int LV or NILV.

298 Altogether, based on a complete set of virological, immunological and histopathological data, the
299 LV::S_{FL} vector elicited anti-S_{CoV-2} NAbs and T-cell responses and provided robust protection against
300 SARS-CoV-2 infection in two pertinent animal models, and particularly when mucosal i.n.
301 administration was included in the vaccinal scheme.

302

303 **Discussion**

304 Prophylactic strategies are necessary to control SARS-CoV-2 infection which, 6 months into the
305 pandemic, still continues to spread exponentially without signs of slowing down. It is now
306 demonstrated that primary infection with SARS-CoV-2 in rhesus macaques leads to protective
307 immunity against re-exposure (Chandrashekar et al., 2020). Numerous vaccine candidates, based on
308 naked DNA (Yu et al., 2020) or mRNA, recombinant protein, replicating or non-replicating viral
309 vectors, including adenoviral Ad5 vector (Zhu et al., 2020), or alum-adjuvanted inactivated virus (Gao
310 et al., 2020) are under active development for COVID-19 prevention. Our immunological rationale for
311 selecting LV to deliver gene encoding S_{CoV-2} antigen was based on its potential to induce in situ
312 expression of heterologous genes, and on the ability of this immunization platform to elicit sustained
313 humoral and cell-mediated responses. Unique to LV is the ability to transduce proliferating as well as
314 non-dividing cells such as dendritic cells (Esslinger et al., 2002; Firat et al., 2002; He et al., 2005),
315 thereby serving as a powerful vaccination strategy (Beignon et al., 2009; Buffa et al., 2006; Coutant et
316 al., 2012; Gallinaro et al., 2018; Iglesias et al., 2006) to provoke strong and long-lasting adaptive
317 responses (Cousin et al., 2019; Ku et al., in revision.). Notably, in net contrast to many other viral
318 vectors, LV do not suffer from pre-existing immunity in populations, due to their pseudo-typing with
319 the glycoprotein envelope from Vesicular Stomatitis Virus, to which humans are barely exposed. We
320 recently demonstrated that a single injection of an LV expressing Zika envelope provides a rapid and
321 durable sterilizing protection against Zika infection (Ku et al., 2020). Our recent comprehensive
322 comparison of LV to the gold standard Ad5 immunization vector also documented the superiority of
323 LV in inducing multifunctional and central memory T-cell responses in the mouse model, and its strong
324 immunogenicity in outbred rats (Ku et al., in revision.), underlining the suitability of LV for vaccinal
325 applications.

326 Because laboratory mice are not naturally susceptible permissive to SARS-CoV-2 infection, we set
327 up an *in vivo* transduction murine model in which the hACE2 expression is induced in the respiratory
328 tracts by an i.n. Ad5::hACE2 pretreatment prior to SARS-CoV-2 inoculation. Our system, very close
329 to a recently published protocol (Sun et al., 2020) confirmed that mice become largely permissive to
330 SARS-CoV-2 replication in the lungs and thus represent a model for assessment of vaccine or drug
331 efficacy against this virus. Even though the Ad5::hACE2 model may not fully mimic the physiological
332 ACE2 expression profile and thus may not reflect all the aspects of the pathophysiology of SARS-
333 CoV-2 infection, it provides a pertinent model to evaluate *in vivo* the effects of anti-viral drugs, vaccine
334 candidates, various mutations or genetic backgrounds on the SARS-CoV-2 replication. By using a low
335 dose of Ad5::hACE2, no $CD45^+$ cell recruitments were detectable at day 4 post instillation, indicative
336 of an absence of Ad5-related inflammation before the inoculation of SARS-CoV-2.

337 We first evaluated the efficacy of several LV each encoding for one of the variants of S, i.e., the S1
338 domain alone (LV::S1), the S1-S2 ecto-domain, devoid of the transmembrane and C-terminal short
339 internal tail (LV::S1-S2), or full-length, membrane anchored protein (LV::S_{FL}). Even though a single
340 administration of each of these LV was able to induce high anti-S_{CoV-2} Ab titers, only LV::S_{FL} induced
341 highly functional Nabs with neutralizing activities similar to those found in a cohort of symptomatic
342 SARS-CoV-2 patients. This finding predicted a protective potential of the humoral responses induced
343 by the LV::S_{FL} vector. In addition, strong anti-S_{CoV-2} $CD8^+$ T-cell responses were also observed in the
344 spleen of mice as early as 2 weeks after a single LV::S_{FL} injection, as detected against numerous MHC-
345 I-restricted immunogenic regions that we identified in C57BL/6 (H-2^b) mice.

346 In the transduced mouse model which allows high rates of SARS-CoV-2 replication, vaccination by
347 a single i.p. administration of 1 x 10^7 TU of LV::S_{FL}, 6 weeks before virus inoculation, was sufficient
348 to inhibit the viral replication by ~ 6 folds. Further boosting via the systemic route did not afford
349 improved protection rate when compared to a single administration. However, systemic priming
350 followed by a mucosal boost inhibited efficiently viral replication and prevented lung inflammation.
351 This protection was correlated with high titers of anti-S_{CoV-2} IgG and IgA and a strong neutralization
352 activity in sera. Additional experiments in appropriate transgenic mice or adoptive immune cell transfer
353 approaches will be necessary to identify the immunological pathways that contribute to disease severity
354 or protection against SARS-CoV-2. NAbs and cell-mediated immunity, very efficaciously induced
355 with the LV-based vaccine candidate, may synergize to block infection and viral replication.

356 *M. auratus* golden hamsters are naturally permissive to SARS-CoV-2 replication and recapitulate
357 the human COVID-19 physiopathology (Sia et al., 2020). In hamsters immunized with the prime-target
358 regimen, either with integrative LV or NILV::S_{FL}, we observed substantial degrees of protection
359 against SARS-CoV-2, as judged by: (i) the drastic reduction of the lung viral loads (determined by
360 qRT-PCR) or infectious particle clearance (determined by PFU assay), (ii) the significant reduction in
361 the expression of inflammatory mediators in the lung, and (iii) the efficient prevention of lung tissue
362 damage. Confirmation, in this highly sensitive species, of the protection results further supports the
363 LV::S_{FL} vaccine, especially in its non-integrative form, as a candidate for future introduction into
364 clinical trials.

365 Ab-Dependent Enhancement (ADE) of coronavirus entry to the host cells has been evoked as a
366 potential obstacle in vaccination against coronaviruses. With DNA (Yu et al., 2020) or inactivated
367 SARS-CoV-2 virus (Gao et al., 2020) vaccination in macaques, no immunopathological exacerbation
368 has been observed. Long term observation even after decrease in Ab titer could be necessary to exclude
369 such hypothesis. In the case of MERS-CoV, it has been reported that one particular RBD-specific
370 neutralizing monoclonal Ab (Mersmab1) could mediate in vitro ADE of MERS-CoV into the host cells
371 by mimicking the viral receptor human DPP4 and inducing conformational rearrangements of S_{MERS}

372 (Wan et al., 2020). We believe that it is difficult to compare the polyclonal Ab response and its paratope
373 repertoire complexity with the singular properties of a monoclonal Ab which cannot be representative
374 of the polyclonal response induced by a vaccine. In addition, very contradictorily, results from the same
375 team reported that a single-dose treatment with a humanized version of Mersmab1 afforded complete
376 protection of a human transgenic mouse model from lethal MERS challenge (Qiu et al., 2016).
377 Therefore, even with an Ab which might facilitate the cell host invasion in vitro in some conditions,
378 not only there is no exacerbation of the infection in vivo, but also there is a notable protection.

379 It is noteworthy that all vaccine candidates currently under clinical development are planned to be
380 administered via the i.m. route and will thus induce systemic - but not mucosal - immunity. Our results
381 evidenced a strong correlation between the presence of mucosal anti-S_{CoV-2} IgA, local NAb activity in
382 the respiratory tracts and very robust pulmonary protection. Therefore, vaccine administration via the
383 i.n. route, which is the main entry door of SARS-CoV-2, has to be taken into the account when
384 establishing the COVID-19 vaccination protocols, especially since this route is non-invasive and
385 particularly suitable for mass vaccination of children and elderly people.

386 The fact that the current vaccine candidates do not take advantage of i.n. immunization is certainly
387 related to the pro-inflammatory properties of most of the vaccination vectors or the requirement of
388 encapsulation/adjuvantation of nucleic acids or inactivated vaccines, which rise safety concerns.
389 Unlike most of the other vaccination viral vectors, LV are non-replicative, non-inflammatory, do not
390 suffer from pre-existing immunity in human populations, and are effective under their non-integrative
391 variant. Therefore, LV are particularly safe and favorable for use in mucosal immunization through the
392 i.n. route, which is essential in immune protection against SARS-CoV-2. Prophylactic vaccination is
393 the most cost-effective and efficient strategy against infectious diseases in general and against
394 emerging coronaviruses in particular. Our results firmly established that the LV encoding for S_{CoV-2},
395 used in a prime-target protocol is a prominent vaccine strategy against COVID-19.

396 **Acknowledgments**

397 The authors are grateful to Pr Sylvie van der Werf (National Reference Centre for Respiratory
398 Viruses hosted by Institut Pasteur, Paris, France) for providing the BetaCoV/France/IDF0372/2020
399 SARS-CoV-2 clinical isolate. The strain BetaCoV/France/IDF0372/2020 was supplied through the
400 European Virus Archive goes Global (Evag) platform, a project that has received funding from the
401 European Union's Horizon 2020 research and innovation program under grant agreement No 653316.
402 The authors thank Dr Cyril Planchais for the preparation of recombinant homotrimeric S, S1 and RBD
403 proteins and Damien Batalie for excellent technical assistance in determination of viral loads. The
404 preparation of histological sections was performed gratuitously by HISTALIM (Part of Cerba Research
405 - Biomarkers Division, Montpellier, France).

406 This work is also supported by grants from Institut Pasteur, TheraVectys and Agence Nationale de
407 la Recherche (ANR) HuMoCID. Min Wen Ku is part of the Pasteur - Paris University (PPU)
408 International PhD Program and received funding from the Institut Carnot Pasteur Microbes & Santé,
409 and the European Union's Horizon 2020 research and innovation program under the Marie
410 Sklodowska-Curie grant agreement No 665807.

411 **Author Contribution**

412 Study concept and design: MWK, MB, FA, AM, NE, LM, PC, acquisition of data: MWK, MB, PA,
413 JL, KN, BV, FN, PS, HT, ES, FA, AM, LM, construction and production of LV and technical support:
414 PA, FM, AN, FN, CB, PS, analysis and interpretation of data: MWK, MB, PA, JL, KN, FA, AM, NE,
415 LM, PC, histology: MLD, FG, LF, recombinant S proteins: HM, drafting of the manuscript: MWK,
416 MB, FG, LM, PC.

417 **Declaration of Interests**

418 PC is the founder and CSO of TheraVectys. Other authors declare no competing interests.

419

420 **Figure Legend**

421 **Figure 1. Induction of anti-S_{CoV-2} Ab responses by LV. (A)** Schematic representation of 3 forms
422 of S_{CoV-2} protein (S_{FL}, S1-S2 and S1) encoded by LV injected to mice. RBD, S1/S2 and S2' cleavage
423 sites, Fusion Peptide (FP), TransMembrane (TM) and short internal tail (T) are indicated. **(B)** Dynamic
424 of anti-S_{CoV-2} Ab response following LV immunization. C57BL/6 mice (*n* = 4/group) were injected i.p.
425 with 1×10^7 TU of LV::GFP as a negative control, LV::S1, LV::S1-S2, or LV::S_{FL}. Sera were collected
426 at 2, 3, 4 and 6 weeks post immunization. Anti-S_{CoV-2} IgG responses were evaluated by ELISA and
427 expressed as mean endpoint dilution titers. **(C)** Neutralization capacity of anti-S_{CoV-2} Abs induced by
428 LV::S_{FL} immunization. Mouse sera were evaluated in a sero-neutralization assay to determine 50%
429 effective concentration (EC50) neutralizing titers. **(D)** Correlation between the Ab titers and
430 neutralization activity in various experimental groups. Statistical significance was determined by two-
431 sided Spearman rank-correlation test. NS: not significant. **(E)** Head-to-head comparison at a 1:40
432 dilution between mouse sera taken at weeks 3 or 4 after immunization and a cohort of mildly
433 symptomatic individuals living in Crépy-en-Valois, Ile de France. These patients did not seek medical
434 attention and recovered from COVID-19. Results are expressed as mean ± SEM percentages of
435 inhibition of luciferase activity. See also Figure S1.

436 **Figure 2. Induction of T-cell responses by LV::S_{FL}.** C57BL/6 mice (*n* = 3) were immunized i.p.
437 with 1×10^7 TU of LV::S_{FL} or a negative control LV. **(A)** Splenocytes collected 2 weeks after
438 immunization were subjected to an IFN-γ ELISPOT using 16 distinct pools of 15-mer peptides
439 spanning the entire S_{CoV-2} (1-1273 a.a.) and overlapping each other by 10 a.a. residues. SFU = Spot-
440 Forming Cells. **(B)** Deconvolution of the 16 positive peptide pools by ELISPOT applied to splenocytes
441 pooled from 3 LV::S_{FL}-or Ctrl LV-immunized mice. **(C)** Intracellular IFN-γ *versus* IL-2 staining of
442 $CD4^+$ or $CD8^+$ T splenocytes after stimulation with individual peptides encompassing the
443 immuodominant epitopes.

444 **Figure 3. Set up of a murine model expressing hACE2 in the respiratory tracts. (A)** Detection
445 of hACE2 expression by RT-PCR in HEK293 T cells transduced with Ad5::hACE2, at 2 days post
446 transduction. NT: Not transduced. **(B)** hACE2 protein detection by Western Blot in lung cell extracts
447 recovered at day 4 after i.n. instillation of Ad5::hACE2 or empty Ad5 to C57BL/6 mice (*n* = 2/group).
448 **(C)** GFP expression in lung cells prepared at day 4 after i.n. instillation of Ad5::GFP or PBS into
449 C57BL/6 mice, as assessed by flow cytometry in the $CD45^+$ hematopoietic or $EpCam^+$ epithelial cells.
450 **(D)** Lung viral loads in mice pretreated with 2.5×10^9 IGU of Ad5::hACE2, control empty Ad5 or PBS
451 followed by i.n. inoculation of 1×10^5 $TCID_{50}$ of SARS-CoV-2 4 days later. In one group, the
452 Ad5::hACE2-pretreated mice were inoculated with an equivalent amounts of heat-killed (HK) virus to
453 measure the input viral RNA in the absence of viral replication. Viral load quantitation by qRT-PCR
454 in the lung homogenates at 2, 4 or 7 dpi. The red line indicates the detection limit. **(E)** Percentages of

455 $CD45^+$ cells in the lungs, as determined 4 days after pretreatment with various doses of Ad5::hACE2.
456 **(F)** Lung viral loads in mice pretreated with various doses of Ad5::hACE2, followed by i.n. inoculation
457 of 1×10^5 $TCID_{50}$ of SARS-CoV-2 4 days later. Viral load were determined at 3 dpi. See also Figure
458 S2.

459 **Figure 4. Intranasal boost with LV::S_{FL} strongly protects against SARS-CoV-2 in mice. (A)**
460 Timeline of the prime-boost strategy based on LV, followed by Ad5::hACE2 pretreatment and SARS-
461 CoV-2 challenge. **(B)** Titers of anti-S_{CoV-2} IgG, as quantitated by ELISA in the sera of C57BL/6 mice
462 primed i.p. at week 0 and boosted i.p. or i.n. at week 3 (left). Titers were determined as mean endpoint
463 dilution before boost (week 3) and challenge (week 4). *** p <0.001, **** p <0.0001; two-way ANOVA
464 followed by Sidak's multiple comparison test. NS, not significant. Neutralization capacity of these sera,
465 indicated as EC50 (right). See also Figure S4A. **(C)**. Lung viral loads at 3 dpi in mice primed (i.p.) and
466 boosted (i.p. or i.n.) with LV::S_{FL}. Sham-vaccinated received an empty LV. The red line indicates the
467 detection limit. Statistical significance of the differences in the viral loads was evaluated by two tailed
468 unpaired t test; * = p <0.0139, *** = p <0.0088. **(D)** Titers of anti-S_{CoV-2} IgG and IgA Abs determined in
469 the clarified lung homogenates by ELISA, by use of a foldon-trimerized S_{CoV-2} for coating. See also
470 Figure S4B. **(E)** Neutralizing activity of the clarified lung homogenates, determined for 1/5 dilution.
471 Statistical significance of the difference was evaluated by Mann-Whitney U test (*= p <0.0159).

472 **Figure 5. LV::S_{FL} vaccination reduces SARS-Co-2-mediated lung inflammation in mice. (A)**
473 Gating strategy applied to total lung cells to quantitate innate immune subsets. **(B)** Percentages of each
474 innate immune subset versus total lung $CD45^+$ cells at 3 dpi in mice sham-vaccinated or vaccinated
475 with LV::S_{FL}, following various prime-boost regimen compared to non-infected (NI) controls which
476 only received PBS. All mice were pretreated with Ad5::hACE-2, 4 days prior to SARS-CoV-2
477 inoculation. **(C)** Relative log_2 fold change in cytokines and chemokines mRNA expression in mice
478 sham-vaccinated or vaccinated with LV::S_{FL}, following various prime-boost regimen at 3 dpi. Data
479 were normalized versus PBS-treated, unchallenged controls. Statistical significance of the differences in
480 cytokines and chemokines level was evaluated by one-way ANOVA; * = p<0.05, ** = p <0.01. See also
481 Figure S5A-C.

482 **Figure 6. Intranasal vaccination with LV::S_{FL} strongly protects against SARS-CoV-2 in**
483 **golden hamsters. (A)** Timeline of the LV::S_{FL} prime-boost/target immunization regimen and SARS-
484 CoV-2 challenge in hamsters. Sham-vaccinated received an empty LV. **(B)** Dynamic of anti-S_{CoV-2} Ab
485 response following LV immunization. Sera were collected from sham- or LV-vaccinated hamsters at
486 3, 5 (pre-boost), and 6 (post-boost) weeks after the prime injection. Anti-S_{CoV-2} IgG responses were
487 evaluated by ELISA and expressed as mean endpoint dilution titers. **(C)** Post boost/target EC50
488 neutralizing titers, determined in the hamsters' sera after boost, and as compared to the sera from a
489 cohort of asymptomatic (AS), pauci-symptomatic (PS), symptomatic COVID-19 cases (S) or healthy

490 contacts (H) in humans. **(D)** Weight follow-up in hamsters, either sham- or LV::S_{FL}-vaccinated with
491 diverse regimens. For further clarity, only the individuals reaching 4 dpi are shown. Those sacrificed
492 at 2 dpi had the same mean weight as their counterparts of the same groups between 0 and 2 dpi. **(E)**
493 Lung viral loads at 2 or 4 dpi with SARS-CoV-2 in LV::S_{FL}-vaccinated hamsters. Statistical significance
494 of the differences in the viral loads was evaluated by two tailed unpaired t test; * = p<0.0402, **** = p
495 <0.0001. **(F)** Lung viral infectious particles, quantified as PFU at 2 or 4 dpi. The red lines indicate the
496 detection limit of the qRT-PCR or PFU assay.

497 **Figure 7. LV::S_{FL} vaccination reduces SARS-Co-2-mediated lung inflammation and**
498 **histopathology in golden hamsters.** Animals are those detailed in the Figure 6. **(A)** Relative log_2 fold
499 changes in cytokines and chemokines expression in LV::S_{FL}-vaccinated and protected hamsters versus
500 unprotected sham-vaccinated individuals, as determined at 4 dpi by qRT-PCR in the total lung
501 homogenates and normalized versus untreated controls. Statistical significance of the differences in
502 cytokines and chemokines level was evaluated by one-way ANOVA; * = p<0.05, ** = p <0.01. See also
503 Figure S6. **(B)** Histological analysis HE&S lung shown for 2 and 4 dpi. Original magnification: x10,
504 scale bar: 100 µm. Br: Bronchi or bronchiole. Bv: Blood vessel. Arrow: Mononuclear inflammatory
505 cell infiltration. Star: Degenerative changes in the respiratory epithelium. **(C)** Heatmap recapitulating
506 the average of histological scores, for each defined parameter and determined for individuals of the
507 same groups at 2 or 4 dpi.

508 **Methods**

509 **Construction of transfer pFLAP plasmids coding for S_{FL}, S1-S2, or S1 proteins**

510 A codon-optimized full-length S (1-1273) sequence was amplified from pMK-RQ_S-2019-nCoV
511 and inserted between BamHI and XhoI sites of pFlap-ieCMV-WPREm. Sequences encoding for S1-
512 S2 (1-1211) or S1 (1-681) were amplified by PCR from the pFlap-ieCMV- S_{FL}-WPREm plasmid and
513 sub-cloned into pFlap-ieCMV-WPREm between the BamHI and XhoI restriction sites (Figure S1).
514 Each of the PCR products were inserted between the native human ieCMV promoter and a mutated
515 Woodchuck Posttranscriptional Regulatory Element (mWPRE) sequence, in which the *atg* starting
516 codon was mutated to avoid transcription of the downstream truncated "X" protein of Woodchuck
517 Hepatitis Virus, in order to improve the vector safety. Plasmids were amplified in *Escherichia coli*
518 DH5a in Lysogeny Broth supplemented with 50 µg/ml of kanamycin and purified using the
519 NucleoBond Xtra Maxi EF Kit (Macherey Nagel) and resuspended in Tris-EDTA Endotoxin-Free
520 buffer overnight. Plasmid were quantified with a NanoDrop 2000c spectrophotometer (Thermo Ficher,
521 Illkirch, France), aliquoted and stored at -20°C. Plasmid DNA were verified by enzymatic digestion
522 and by sequencing the region proximal to the transgene insertion sites.

523 **Production and titration of LV**

524 Non-replicative LV were produced in Human Embryonic Kidney (HEK)-293T cells, as previously
525 detailed (Zennou et al., 2000). Briefly, lentiviral particles were produced by transient calcium
526 phosphate co-transfection of HEK293T cells with the vector plasmid pTRIP/sE, a VSV-G Indiana
527 envelope plasmid and an encapsidation plasmid (p8.74 or pD64V for the production of integration-
528 proficient or integration-deficient vectors respectively). Supernatants were harvested at 48h post
529 transfection, clarified by 6-minute centrifugation at 2500 rpm at 4°C. LV were aliquoted and stored at
530 -80°C. Vector titers were determined by transducing 293T cells treated with aphidicolin. The titer,
531 proportional to the efficacy of nuclear gene transfer, is determined as Transduction Unit (TU)/ml by
532 qPCR on total lysates at day 3 post transduction, by use of forward 5'-TGG AGG AGG AGA TAT
533 GAG GG-3' and reverse 5'-CTG CTG CAC TAT ACC AGA CA-3' primers, specific to pFLAP
534 plasmid and forward 5'-TCT CCT CTG ACT TCA ACA GC-3' and reverse 5'-CCC TGC ACT TTT
535 TAA GAG CC-3' primers specific to the host housekeeping gene *gadph* as previously described
536 (Iglesias et al., 2006).

537 **Mouse and hamster studies**

538 Female C57BL/6JRj mice (Janvier, Le Genest Saint Isle, France) were used between the age of 6
539 and 10 weeks. Male *Mesocricetus auratus* golden hamsters (Janvier, Le Genest Saint Isle, France) were
540 purchased mature, i.e. 80-90 gr weight. At the beginning of the immunization regimen they weighed
541 100 to 120 gr. Experimentation on animals was performed in accordance with the European and French

542 guidelines (Directive 86/609/CEE and Decree 87-848 of 19 October 1987) subsequent to approval by
543 the Institut Pasteur Safety, Animal Care and Use Committee, protocol agreement delivered by local
544 ethical committee (CETEA #DAP20007) and Ministry of High Education and Research
545 APAFIS#24627-2020031117362508 v1. Animals were vaccinated with the indicated TU of LV and
546 sera were collected at various time points post immunization to monitor binding and neutralization
547 activities. Previous to i.m. or i.n. instillations, animals were anesthetized by i.p. injection of a mixture
548 of Ketamine (Imalgene, 50 mg/kg) and Xylazine (Rompun, 50 mg/kg).

549 **SARS-CoV-2 inoculation**

550 Hamsters or Ad5::hACE2-pretreated mice were anesthetized by i.p. injection of mixture Ketamine
551 and Xylazine, transferred into a biosafety cabinet 3 where they were inoculated i.n. with 0.3 or 1×10^5
552 $TCID_{50}$ of the BetaCoV/France/IDF0372/2020 SARS-CoV-2 clinical isolate (Lescure et al., 2020),
553 amplified in VeroE6 cells. The strain BetaCoV/France/IDF0372/2020 was supplied by the National
554 Reference Centre for Respiratory Viruses hosted by Institut Pasteur (Paris, France) and headed by Pr.
555 Sylvie van der Werf. The human sample from which strain BetaCoV/France/IDF0372/2020 was
556 isolated has been provided by Dr. X. Lescure and Pr. Y. Yazdanpanah from the Bichat Hospital, Paris,
557 France. The viral inoculum was contained in 20 µl for mice and in 50 µl for hamsters. Animals were
558 then housed in an isolator in BioSafety Level 3 animal facilities of Institut Pasteur. The organs and
559 fluids recovered from the animals infected with live SARS-CoV-2 were manipulated following the
560 approved standard operating procedures of these facilities.

561 **Recombinant S_{CoV-2} proteins**

562 Codon-optimized nucleotide fragments encoding a stabilized foldon-trimerized version of the
563 SARS-CoV-2 S ectodomain (a.a. 1 to 1208), the S1 monomer (a.a. 16 to 681) and the RBD subdomain
564 (amino acid 331 to 519) both preceded by a murine IgK leader peptide and followed by an 8xHis Tag
565 were synthetized and cloned into pcDNA™3.1/Zeo$^{(+)}$ expression vector (Thermo Fisher). Proteins
566 were produced by transient co-transfection of exponentially growing Freestyle™ 293-F suspension
567 cells (Thermo Fisher) using polyethylenimine (PEI)-precipitation method as previously described
568 (Lorin and Mouquet, 2015). Recombinant S_{CoV-2} proteins were purified by affinity chromatography
569 using the Ni Sepharose® Excel Resin according to manufacturer's instructions (Thermo Fisher).
570 Protein purity was evaluated by in-gel protein silver-staining using Pierce Silver Stain kit (Thermo
571 Fisher) following SDS-PAGE in reducing and non-reducing conditions using NuPAGE™ 3-8% Tris-
572 Acetate gels (Life Technologies). Purified proteins were dialyzed overnight against PBS using Slide-
573 A-Lyzer® dialysis cassettes (10 kDa MW cut-off, Thermo Fisher). Protein concentration was
574 determined using the NanoDrop™ One instrument (Thermo Fisher).

575 **ELISA**

576 Ninety-six-well Nunc Polysorp plates (Nunc, Thermo Ficher) were coated overnight at 4 °C with
577 100 ng/well of purified S_{CoV-2} proteins in carbonate-bicarbonate buffer (pH 9.6). The next day, plates
578 were blocked with carbonate buffer containing 1% BSA for 2 h at 37°C. Wells were then washed with
579 PBS containing 0.05% Tween 20 (PBS-T), 1:100-diluted sera or 1:10-diluted lung homogenates in
580 PBS-T containing 1% BSA and four serial ten-to-ten dilutions were added and incubated during 2h at
581 37°C. After PBS-T washings, plates were incubated with 1,000-fold diluted peroxydase-conjugated
582 goat anti-mouse IgG (Jackson ImmunoResearch Europe Ltd, Cambridgeshire, United Kingdom) for 1
583 h. Plates were revealed by adding 100 µl of 3,3',5,5'-tetramethylbenzidine chromogenic substrate
584 (Eurobio Scientific). Following a 30 min incubation, reaction was stopped by adding 100 µl of 2N
585 H2SO4 and optical densities were measured at 450nm/620nm on a PR3100 reader.

586 **NAb Detection**

587 Serial dilutions of heat inactivated sera or clarified lung homogenates were assessed for NAbs via
588 an inhibition assay which uses HEK293T cells transduced to stably express human ACE2 and non-
589 replicative S_{CoV-2} pseudo-typed LV particles which harbor the reporter *luciferase firefly* gene, allowing
590 quantitation of the host cell invasion by mimicking fusion step of native SARS-CoV-2 virus (Sterlin et
591 al., 2020). First, 1.5×10^2 TU of S_{CoV-2} pseudo-typed LV were pre-incubated, during 30 min at room
592 temperature, in U-bottom plates, with serial dilutions of each serum in a final volume of 50µl in
593 DMEM-glutamax, completed with 10% heat-inactivated FCS and 100 U/ml penicillin and 100 µg/ml
594 streptomycin. The samples were then transferred into clear-flat-bottom 96-well-black-plates (Corning),
595 and each well received 2×10^4 hACE2$^+$ HEK293-T cells, counted in a NucleoCounter NC.200 system
596 (Chemometec, Denmark) contained in 50 µl. After 2 days incubation at 37°C 5% CO_2, the transduction
597 efficiency of hACE2$^+$ HEK293-T cells by pseudo-typed LV particles was determined by measuring
598 the luciferase activity, using a Luciferase Assay System (Promega) on an EnSpire plate reader
599 (PerkinElmer), as detailed elsewhere (Sterlin et al., 2020). Results are expressed as percentages of
600 inhibition of luciferase activity compared to the maximum of luciferase activity in the absence of NAbs.

601 Serum samples from COVID-19 cases have been recently described elsewhere (Grzelak et al.,
602 2020). Each participant provided written consent to participate in the study, which was approved by
603 the regional investigational review board (IRB; Comité de Protection des Personnes Ile-de-France VII,
604 Paris, France), according to European guidelines and the Declaration of Helsinki. The study was
605 registered as ClinicalTrials.gov (NCT04325646).

606 **S_{FL} T-cell epitope mapping**

607 In order to map the immuno-dominant epitopes of S_{CoV-2}, peptides spanning the whole S_{FL}
608 (Mimotopes, Australia) were pooled by 16, each containing 15 a.a. residues overlapping by 10 a.a.

609 Peptides were dissolved in DMSO at a concentration of 2 mg/ml and diluted before use at 1 µg/ml for
610 ELISPOT or 2-5 µg/ml for ICS (Intracellular Cytokine Staining) in RPMI–1640 medium supplemented
611 with 10% FCS, 100 U/ml penicillin, 100 µg/ml streptomycin, 1 x 10^{-4} M non-essential amino-acids,
612 1% vol/vol HEPES, 1 x 10^{-3} M sodium pyruvate and 5 × 10^{-5} M of β-mercapto-ethanol. IFN-γ
613 ELISPOT and ICS assays were performed as described previously (Bourgine et al., 2018; Sayes et al.,
614 2016). For ICS, cells were acquired in an Attune NxT Flow cytometer (Thermo Fisher) and the data
615 were analyzed by FlowJo Software (TreeStar Inc.).

616 **Generation of Ad5 gene transfer vectors**

617 The Ad5 gene transfer vectors were produced using the ViraPower Adenoviral Promoterless
618 Gateway Expression Kit (Thermo Fisher). The sequence containing CMV promoter, BamH1/Xho1
619 restriction sites and WPRE was PCR amplified from the pTRIPΔU3CMV plasmid, by use of: (i)
620 forward primer, encoding the attB1 in the 5' end, and (ii) reverse primer, encoding both the attB2 and
621 SV40 polyA signal sequence in the 5' end. The attB-PCR product was cloned into the gateway
622 pDONR207 donor vector, via BP Clonase reaction. The *hACE2* was amplified from a plasmid
623 derivative of hACE2-expressing pcDNA3.1, while e*gfp* was amplified from pTRIP-ieCMV-eGFP-
624 WPRE (Ku et al., in revision.). The amplified PCR products were cloned into the pDONR207 plasmid
625 via the BamH1 and Xho1 restriction sites. To obtain the final Ad5 plasmid, the pDONR207 vector,
626 harboring *hACE2* or *gfp* genes, was further inserted into pAd/PL-DEST™ vector via LR Clonase
627 reaction (Figure S7).

628 The Ad5 virions were generated by transfecting the E3-transcomplementing HEK-293A cell line
629 with pAd CMV-GFP-WPRE-SV40 polyA or pAd CMV-hACE2-WPRE-SV40 polyA plasmid
630 followed by subsequent vector amplification, according to the manufacturer's protocol (ViraPower
631 Adenoviral Promoterless Gateway Expression Kit, Thermo Fisher). The Ad5 particles were purified
632 using Adeno-X rapid Maxi purification kit and concentrated with the Amicon Ultra-4 10k centrifugal
633 filter unit. Vectors were resuspended and stored à -80°C in PIPES buffer pH 7.5, supplemented with
634 2.5% glucose. Ad5 were titrated using a qPCR protocol, as described (Gallaher and Berk, 2013).

635 **Western blot**

636 Expression of hACE2 in the lungs of Ad5::hACE2-transduced mice was assessed by Western
637 Blotting. One million cells from lung cell suspension were resolved on 4 – 12 % NuPAGE Bis-Tris
638 protein gels (Thermo Fisher), then transferred onto a nitrocellulose membrane (Biorad, France). The
639 nitrocellulose membrane was blocked in 5 % non-fat milk in PBS-T for 2 hours at room temperature
640 and probed overnight with goat anti-hACE2 primary Ab at 1 µg/mL (AF933, R&D systems).
641 Following three wash intervals of 10 minutes with PBS-T, the membrane was incubated for 1 hour at
642 room temperature with HRP-conjugated anti-goat secondary Ab and HRP-conjugated anti-β-actin

643 (ab197277, Abcam). The membrane was washed with PBS-T thrice before visualization with enhanced
644 chemiluminescence via the super signal west femto maximum sensitivity substrate (ThermoFisher) on
645 ChemiDoc XRS+ (Biorad, France). PageRuler Plus prestained protein ladder was used as size
646 reference.

647 **Determination of SARS-CoV-2 viral loads in the lungs**

648 Half of each lung lobes were removed aseptically and frozen at -80°C. Organs were thawed and
649 homogenized for 20 s at 4.0 m/s, using lysing matrix M (MP Biomedical) in 500 µl of ice-cold PBS.
650 The homogenization was performed in an MP Biomedical Fastprep 24 Tissue Homogenizer. The
651 homogenates were centrifuged 10 min at 2000g for further RNA extraction from the supernatants.
652 Particulate viral RNA was extracted from 70 µl of such supernatants using QIAamp Viral RNA Mini
653 Kit (Qiagen) according to the manufacturer's procedure. Viral load was determined following reverse
654 transcription and real-time quantitative TaqMan® PCR essentially as described (Corman et al., 2020),
655 using SuperScript^{TM} III Platinum One-Step Quantitative RT-PCR System (Invitrogen) and primers and
656 probe (Eurofins) targeting S_{CoV-2} gene as listed in Table S1. In vitro transcribed RNA derived from
657 plasmid "pCI/SARS-CoV envelope" was synthesized using T7 RiboMAX Express Large Scale RNA
658 production system (Promega), then purified by phenol/chloroform extractions and two successive
659 precipitations with isopropanol and ethanol. RNA concentration was determined by optical density
660 measurement, then RNA was diluted to 10^9 genome equivalents/µL in RNAse-free water containing
661 100µg/mL tRNA carrier, and stored in single-use aliquots at -80°C. Serial dilutions of this in vitro
662 transcribed RNA were prepared in RNAse-free water containing 10µg/ml tRNA carrier and used to
663 establish a standard curve in each assay. Thermal cycling conditions were: (i) reverse transcription at
664 55°C for 10 min, (ii) enzyme inactivation at 95°C for 3 min, and (iii) 45 cycles of
665 denaturation/amplification at 95°C for 15 s, 58°C for 30 s. Products were analyzed on an ABI 7500
666 Fast real-time PCR system (Applied Biosystems). PFU assay was performed as recently described
667 (Case et al., 2020).

668 **Cytometric analysis of lung cells**

669 Lungs from individual mice were treated with 400 U/ml type IV collagenase and DNase I (Roche)
670 for a 30-minute incubation at 37°C and homogenized by use of GentleMacs (Miltenyi Biotech) mAbs.
671 Cells were filtered through 100 µm-pore filters and centrifuged at 1200 rpm during 8 minutes. Cells
672 were then treated with Red Blood Cell Lysing Buffer (Sigma) and washed twice in PBS. Cells were
673 stained as follows. (i) To detect DC, monocytes, alveolar and interstitial macrophages: Near IR
674 Live/Dead (Invitrogen), FcγII/III receptor blocking anti-CD16/CD32 (BD Biosciences), BV605-anti-
675 CD45 (BD Biosciences), PE-anti-CD11b (eBioscience), PE-Cy7-antiCD11c (eBioscience), BV450-
676 anti-CD64 (BD Biosciences), FITC-anti-CD24 (BD Biosciences), BV711-anti-CD103 (BioLegend),
677 AF700-anti-MHC-II (BioLegend), PerCP-Cy5.5-anti-Ly6C (eBioscience) and APC anti-Ly-6G

678 (Miltenyi) mAbs, (ii) to detect neutrophils or eosinophils: Near IR DL (Invitrogen), FcγII/III receptor
679 blocking anti-CD16/CD32 (BD Biosciences), PerCP-Vio700-anti-CD45 (Miltenyi), APC-anti-CD11b
680 (BD Biosciences), PE-Cy7-anti-CD11c (eBioscience), FITC-anti-CD24 (BD Biosciences), AF700-
681 anti-MHC-II (BioLegend), PE-anti-Ly6G (BioLegend), BV421-anti-Siglec-F (BD Biosciences), (ii) to
682 detect mast cells, basophils, NK: Near IR LD (Invitrogen), BV605-anti-CD45 (BD Biosciences), PE-
683 anti-CD11b (eBioscience), eF450-anti-CD11c (eBioscience), PE-Cy7-anti-CD117 (BD Biosciences),
684 APC-anti-FcεR1 (BioLegend), AF700-anti-NKp46 (BD Biosciences), FITC-anti-CCR3 (BioLegend),
685 without FcγII/III receptor blocking anti-CD16/CD32. Cells were incubated with appropriate mixtures
686 for 25 minutes at 4°C, washed twice in PBS containing 3% FCS and then fixed with Paraformaldehyde
687 4% by an overnight incubation at 4°C. The cells were acquired in an Attune NxT cytometer system
688 (Invitrogen) and data were analyzed by FlowJo software (Treestar, OR, USA).

689 **qRT-PCR Detection of inflammatory cytokines and chemokines in the lungs of the mice and**
690 **hamsters**

691 Lung samples from mice or hamsters were added to lysing matrix D (MP Biomedical) containing 1
692 mL of TRIzol reagent and homogenized at 30 s at 6.0 m/s twice using MP Biomedical Fastprep 24
693 Tissue Homogenizer. Total RNA was extracted using TRIzol reagent (ThermoFisher) according to the
694 manufacturer's procedure. cDNA was synthesized from 4 µg of RNA in the presence of 2.5 µM of
695 oligo(dT) 18 primers, 0.5 mM of deoxyribonucleotides, 2.0 U of RNase Inhibitor and SuperScript IV
696 Reverse Transcriptase (Thermo Fisher) in 20 µl reaction. The real-time PCR was performed on
697 QuantStudio™ 7 Flex Real-Time PCR System (Thermo Fisher). Reactions were performed in
698 triplicates in a final reaction volume of 10 µl containing 5 µl of iQ™ SYBR® Green Supermix (Biorad,
699 France), 4 µl of cDNA diluted 1:15 in DEPC-water and 0.5 µl of each forward and reverse primers at
700 a final concentration of 0.5 µM (Table S2, S3). The following thermal profile was used: a single cycle
701 of polymerase activation for 3 min at 95°C, followed by 40 amplification cycles of 15 sec at 95°C and
702 30 sec 60°C (annealing-extension step). Mice β-globin or hamster ribosomal protein L18 (RLP18) was
703 used as an endogenous reference control to normalize differences in the amount of input nucleic acid.
704 The average C_T values were calculated from the technical replicates for relative quantification of target
705 cytokines/chemokines. The differences in the C_T cytokines/chemokines amplicons and the C_T of the
706 endogenous reference control, termed ΔC_T, were calculated to normalize for differences in the quantity
707 of nucleic acid. The ΔC_T of the experimental condition compared relatively to the PBS-immunized
708 individuals using the comparative $\Delta\Delta C_T$ method. The fold change in gene expression was further
709 calculated using $2^{-\Delta\Delta C_T}$.

710 **Lung Histopathology**

711 Samples from the lung were fixed in formalin for at least 7 days and routinely embedded in paraffin.
712 Five µm thick paraffin sections were stained with Hematoxylin Eosin & Saffron (HE&S). Microscopic
713 changes were qualitatively described and when applicable scored semi-quantitatively, using: (i)
714 distribution qualifiers (i.e., focal, multifocal, locally extensive or diffuse), and (ii) a five-scale severity
715 grade, i.e., 1: minimal, 2: mild, 3: moderate, 4: marked and 5: severe.

716

717 **Supplemental information titles and legends**

718 **Figure S1. Maps of plasmids used for production of LV encoding S_{FL}, S1-S2 or S1 antigens.**

719 **Figure S2. Lung histology in mice pretreated with Ad5::hACE2 and inoculated with SARS-**
720 **CoV-2.** Histological analysis in C57BL/6 mice, pretreated with PBS or Ad5::hACE2, followed by i.n.
721 inoculation of 1×10^5 $TCID_{50}$ of SARS-CoV-2. Analysis was performed at 3 dpi. Lung, HE&S stain,
722 Original magnification: x10, scale bar: 100 µm. Br: Bronchi or bronchiole. Bv: Blood vessel. Arrow:
723 Mononuclear inflammatory cell infiltration.

724 **Figure S3. Protective potential of systemic immunization with LV::S_{FL} against SARS-CoV-2**
725 **in mice. (A)** Timeline of vaccination by a single i.p. injection of LV followed by Ad5::hACE2
726 pretreatment and i.n. SARS-CoV-2 challenge. **(B)** Lung viral loads in unvaccinated mice (PBS),
727 LV::S_{FL}- or sham-vaccinated mice, at 3 dpi. Statistical significance of the differences in the viral loads
728 was evaluated by two tailed unpaired t test; * = p<0.0139.

729 **Figure S4. Serum or lung homogenate Ab responses against RBD or S1. (A)** Titers of anti-S_{CoV-}
730 $_{2}$ IgG, able to bind to S1 or RBD fragments of S_{CoV-2}, as quantitated by ELISA in the sera of C57BL/6
731 mice primed i.p. at week 0 and boosted i.p. or i.n. at week 3. Titers are determined as mean endpoint
732 dilution. **(B)** Titers of anti-S_{CoV-2} IgG and IgA Abs, as determined in the clarified lung homogenates by
733 ELISA using RBD in coating.

734 **Figure S5. Inflammation mediators in the lungs of LV::SFL- or sham-vaccinated and**
735 **challenged mice.** Relative log_2 fold change in cytokine and chemokine mRNA expression in the
736 challenged "LV::SFL i.p.-i.p." or "LV::SFL i.p.-i.n." groups, as determined by qRT-PCR, applied to
737 total lung homogenates prepared at 3 dpi. Relative expressions are normalized to the mean values
738 obtained in PBS-treated unchallenged controls. Shown are inflammatory mediators: **(A)** significantly
739 unchanged between the "LV::SFL i.p.-i.n." and "sham i.p.-i.n." groups, **(B)** significantly different
740 between "LV::SFL i.p.-i.p." and "sham i.p.-i.p." groups, and **(C)** significantly unchanged between
741 "LV::SFL i.p.-i.p." and "sham i.p.-i.p." groups. Statistical significance was evaluated by two tailed
742 unpaired t test; * = p<0.05, ** = p<0.01, *** = p<0.001 and **** = p <0.0001.

743 **Figure S6. Inflammation mediators in the lungs of LV::S_{FL}- or sham-vaccinated and**
744 **challenged hamsters.** Relative log_2 fold changes in cytokines and chemokines mRNA expression in
745 LV::S_{FL}-vaccinated and protected hamsters versus unprotected sham-vaccinated individuals, as
746 determined at 4 dpi by qRT-PCR in the total lung homogenates and normalized to the mean of untreated
747 controls. Shown are the inflammatory mediators for which the differences between the LV::S_{FL}- and
748 sham-vaccinated hamsters were not statistically different, as evaluated by one-way ANOVA.

749 **Figure S7. Maps of plasmids used for production of Ad5 encoding hACE2.**

750 **Table S1. Sequences of primers and probes for SARS-CoV-2 viral load determination.**

751 **Table S2. Sequences of primers used to quantitate mouse cytokines and chemokines by qRT-**
752 **PCR.**

753 **Table S3. Sequences of primers used to quantitate cytokines, chemokines and transcription**
754 **factor in Syrian golden hamsters.by qRT-PCR.**

755

756 **References**

757 Amanat, F., and Krammer, F. (2020). SARS-CoV-2 Vaccines: Status Report. Immunity *52*, 583-589.

758 Beignon, A.S., Mollier, K., Liard, C., Coutant, F., Munier, S., Riviere, J., Souque, P., and Charneau,
759 P. (2009). Lentiviral vector-based prime/boost vaccination against AIDS: pilot study shows protection
760 against Simian immunodeficiency virus SIVmac251 challenge in macaques. J Virol *83*, 10963-10974.

761 Belouzard, S., Chu, V.C., and Whittaker, G.R. (2009). Activation of the SARS coronavirus spike
762 protein via sequential proteolytic cleavage at two distinct sites. Proc Natl Acad Sci U S A *106*, 5871-
763 5876.

764 Bourgine, M., Crabe, S., Lobaina, Y., Guillen, G., Aguilar, J.C., and Michel, M.L. (2018). Nasal route
765 favors the induction of CD4+ T cell responses in the liver of HBV-carrier mice immunized with a
766 recombinant hepatitis B surface- and core-based therapeutic vaccine. Antiviral Res *153*, 23-32.

767 Buffa, V., Negri, D.R., Leone, P., Borghi, M., Bona, R., Michelini, Z., Compagnoni, D., Sgadari, C.,
768 Ensoli, B., and Cara, A. (2006). Evaluation of a self-inactivating lentiviral vector expressing simian
769 immunodeficiency virus gag for induction of specific immune responses in vitro and in vivo. Viral
770 Immunol *19*, 690-701.

771 Case, J.B., Baileyb, A.L., Kimab, A.S., Chenab, R.E., and Diamond, M.S. (2020). Growth, detection,
772 quatification, and inactivation od SARS-CoV-2. Virology *548*, 39-48.

773 Chandrashekar, A., Liu, J., Martinot, A.J., McMahan, K., Mercado, N.B., Peter, L., Tostanoski, L.H.,
774 Yu, J., Maliga, Z., Nekorchuk, M.*, et al.* (2020). SARS-CoV-2 infection protects against rechallenge
775 in rhesus macaques. Science. May 2020:eabc4776. doi: 10.1126/science.abc4776. PMID: 32434946.

776 Corman, V., Bleicker, T., Brünink, S., and Drosten, C. (2020). Diagnostic detection of 2019-nCoV by
777 real-time RT-PCR. https://www.who.int/docs/default-source/coronaviruse/protocol-v2-1.pdf.

778 Cousin, C., Oberkampf, M., Felix, T., Rosenbaum, P., Weil, R., Fabrega, S., Morante, V., Negri, D.,
779 Cara, A., Dadaglio, G., and Leclerc, C. (2019). Persistence of Integrase-Deficient Lentiviral Vectors
780 Correlates with the Induction of STING-Independent CD8(+) T Cell Responses. Cell Rep *26*, 1242-
781 1257 e1247.

782 Coutant, F., Sanchez David, R.Y., Felix, T., Boulay, A., Caleechurn, L., Souque, P., Thouvenot, C.,
783 Bourgouin, C., Beignon, A.S., and Charneau, P. (2012). A nonintegrative lentiviral vector-based
784 vaccine provides long-term sterile protection against malaria. PLoS One *7*, e48644.

785 Coutard, B., Valle, C., de Lamballerie, X., Canard, B., Seidah, N.G., and Decroly, E. (2020). The spike
786 glycoprotein of the new coronavirus 2019-nCoV contains a furin-like cleavage site absent in CoV of
787 the same clade. Antiviral Res *176*, 104742.

788 Di Nunzio, F., Felix, T., Arhel, N.J., Nisole, S., Charneau, P., and Beignon, A.S. (2012). HIV-derived
789 vectors for therapy and vaccination against HIV. Vaccine *30*, 2499-2509.

790 Esslinger, C., Romero, P., and MacDonald, H.R. (2002). Efficient transduction of dendritic cells and
791 induction of a T-cell response by third-generation lentivectors. Hum Gene Ther *13*, 1091-1100.

792 Firat, H., Zennou, V., Garcia-Pons, F., Ginhoux, F., Cochet, M., Danos, O., Lemonnier, F.A.,
793 Langlade-Demoyen, P., and Charneau, P. (2002). Use of a lentiviral flap vector for induction of CTL
794 immunity against melanoma. Perspectives for immunotherapy. J Gene Med *4*, 38-45.

795 Gallaher, S.D., and Berk, A.J. (2013). A rapid Q-PCR titration protocol for adenovirus and helper-
796 dependent adenovirus vectors that produces biologically relevant results. J Virol Methods *192*, 28-38.

797 Gallinaro, A., Borghi, M., Bona, R., Grasso, F., Calzoletti, L., Palladino, L., Cecchetti, S., Vescio,
798 M.F., Macchia, D., Morante, V., *et al.* (2018). Integrase Defective Lentiviral Vector as a Vaccine
799 Platform for Delivering Influenza Antigens. Front Immunol *9*, 171.

800 Gao, Q., Bao, L., Mao, H., Wang, L., Xu, K., Yang, M., Li, Y., Zhu, L., Wang, N., Lv, Z., *et al.* (2020).
801 Rapid development of an inactivated vaccine candidate for SARS-CoV-2. Science. 2020 Jul
802 3;369(6499):77-81. doi: 10.1126/science.abc1932. Epub 2020 May 6.PMID: 32376603.

803 Grzelak, L., Temmam, S., Planchais, C., Demeret, C., Tondeur, L., Huon, C., Guivel-Benhassine, F.,
804 Staropoli, I., Chazal, M., Dufloo, J., *et al.* (2020). A comparison of four serological assays for detecting
805 anti-SARS-CoV-2 antibodies in human serum samples from different populations. Sci Transl Med.

806 Guo, Y.R., Cao, Q.D., Hong, Z.S., Tan, Y.Y., Chen, S.D., Jin, H.J., Tan, K.S., Wang, D.Y., and Yan,
807 Y. (2020). The origin, transmission and clinical therapies on coronavirus disease 2019 (COVID-19)
808 outbreak - an update on the status. Mil Med Res *7*, 11.

809 He, Y., Zhang, J., Mi, Z., Robbins, P., and Falo, L.D., Jr. (2005). Immunization with lentiviral vector-
810 transduced dendritic cells induces strong and long-lasting T cell responses and therapeutic immunity.
811 J Immunol *174*, 3808-3817.

812 Hobernik, D., and Bros, M. (2018). DNA Vaccines-How Far From Clinical Use? Int J Mol Sci *19*.

813 Hu, B., Tai, A., and Wang, P. (2011). Immunization delivered by lentiviral vectors for cancer and
814 infectious diseases. Immunol Rev *239*, 45-61.

815 Iglesias, M.C., Frenkiel, M.P., Mollier, K., Souque, P., Despres, P., and Charneau, P. (2006). A single
816 immunization with a minute dose of a lentiviral vector-based vaccine is highly effective at eliciting
817 protective humoral immunity against West Nile virus. J Gene Med *8*, 265-274.

818 Ku, M.W., Anna, F., Souque, F., Petres, S., Prot, M., Simon-Loriere, E., Charneau, P., and Bourgine,
819 M. (2020). A Single Dose of NILV-Based Vaccine Provides Rapid and Durable Protection against
820 Zika Virus. Mol Ther. 2020 May 20;S1525-0016(20)30250-1. doi: 10.1016/j.ymthe.2020.05.016.

821 Ku, M.W., Authié, P., Souque, P., Bourgine, M., Romano, M., Charneau, P., and Majlessi, L. (in
822 revision.). High-Quality Memory T Cells by Programmed Antigen Expression in Dendritic Cells
823 Induced by Lentiviral Vector.

824 Lai, A.L., Millet, J.K., Daniel, S., Freed, J.H., and Whittaker, G.R. (2017). The SARS-CoV Fusion
825 Peptide Forms an Extended Bipartite Fusion Platform that Perturbs Membrane Order in a Calcium-
826 Dependent Manner. J Mol Biol *429*, 3875-3892.

827 Lescure, F.X., Bouadma, L., Nguyen, D., Parisey, M., Wicky, P.H., Behillil, S., Gaymard, A.,
828 Bouscambert-Duchamp, M., Donati, F., Le Hingrat, Q.*, et al.* (2020). Clinical and virological data of
829 the first cases of COVID-19 in Europe: a case series. Lancet Infect Dis *20*, 697-706.

830 Lopez, J., Anna, F., Authié, P., Pawlik, A., Ku, M.W., Blanc, C., Souque, P., Moncoq, F., Noirat, A.,
831 Sougakoff, W.*, et al.* (in preparation). An Optimized Poly-antigenic Lentiviral Vector Induces
832 Protective CD4+ T-Cell Immunity and Predicts a Booster Vaccine against Mycobacterium
833 tuberculosis.

834 Lorin, V., and Mouquet, H. (2015). Efficient generation of human IgA monoclonal antibodies. J
835 Immunol Methods *422*, 102-110.

836 Qiu, H., Sun, S., Xiao, H., Feng, J., Guo, Y., Tai, W., Wang, Y., Du, L., Zhao, G., and Zhou, Y. (2016).
837 Single-dose treatment with a humanized neutralizing antibody affords full protection of a human
838 transgenic mouse model from lethal Middle East respiratory syndrome (MERS)-coronavirus infection.
839 Antiviral Res *132*, 141-148.

840 Rosenberg, S.A., Zhai, Y., Yang, J.C., Schwartzentruber, D.J., Hwu, P., Marincola, F.M., Topalian,
841 S.L., Restifo, N.P., Seipp, C.A., Einhorn, J.H.*, et al.* (1998). Immunizing patients with metastatic

842 melanoma using recombinant adenoviruses encoding MART-1 or gp100 melanoma antigens. J Natl
843 Cancer Inst *90*, 1894-1900.

844 Sayes, F., Pawlik, A., Frigui, W., Groschel, M.I., Crommelynck, S., Fayolle, C., Cia, F., Bancroft, G.J.,
845 Bottai, D., Leclerc, C., *et al.* (2016). CD4+ T Cells Recognizing PE/PPE Antigens Directly or via Cross
846 Reactivity Are Protective against Pulmonary Mycobacterium tuberculosis Infection. PLoS Pathog *12*,
847 e1005770.

848 Schirmbeck, R., Reimann, J., Kochanek, S., and Kreppel, F. (2008). The immunogenicity of adenovirus
849 vectors limits the multispecificity of CD8 T-cell responses to vector-encoded transgenic antigens. Mol
850 Ther *16*, 1609-1616.

851 Sia, S.F., Yan, L.M., Chin, A.W.H., Fung, K., Choy, K.T., Wong, A.Y.L., Kaewpreedee, P., Perera,
852 R., Poon, L.L.M., Nicholls, J.M., *et al.* (2020). Pathogenesis and transmission of SARS-CoV-2 in
853 golden hamsters. Nature. 2020 May 14. doi: 10.1038/s41586-020-2342-5. Online ahead of print.PMID:
854 32408338.

855 Sterlin, D., Mathian, A., Miyara, M., Mohr, A., Anna, F., Claër, L., Quentric, P., Fadlallah, J., Ghillani,
856 P., Gunn, C., *et al.* (2020). IgA dominates the early neutralizing antibody response to SARS-CoV-2.
857 https://www.medrxiv.org/content/10.1101/2020.06.10.20126532v1.

858 Sun, J., Zhuang, Z., Zheng, J., Li, K., Wong, R.L., Liu, D., Huang, J., He, J., Zhu, A., Zhao, J., *et al.*
859 (2020). Generation of a Broadly Useful Model for COVID-19 Pathogenesis, Vaccination, and
860 Treatment. Cell *182*, 734-743 e735.

861 Vabret, N., Britton, G.J., Gruber, C., Hegde, S., Kim, J., Kuksin, M., Levantovsky, R., Malle, L.,
862 Moreira, A., Park, M.D., *et al.* (2020). Immunology of COVID-19: Current State of the Science.
863 Immunity *52*, 910-941.

864 Walls, A.C., Park, Y.J., Tortorici, M.A., Wall, A., McGuire, A.T., and Veesler, D. (2020). Structure,
865 Function, and Antigenicity of the SARS-CoV-2 Spike Glycoprotein. Cell *181*, 281-292 e286.

866 Wan, Y., Shang, J., Sun, S., Tai, W., Chen, J., Geng, Q., He, L., Chen, Y., Wu, J., Shi, Z., *et al.* (2020).
867 Molecular Mechanism for Antibody-Dependent Enhancement of Coronavirus Entry. J Virol *94*.

868 Wang, Q., Qiu, Y., Li, J.Y., Zhou, Z.J., Liao, C.H., and Ge, X.Y. (2020). A Unique Protease Cleavage
869 Site Predicted in the Spike Protein of the Novel Pneumonia Coronavirus (2019-nCoV) Potentially
870 Related to Viral Transmissibility. Virol Sin. 2020 Jun;35(3):337-339. doi: 10.1007/s12250-020-00212-
871 7. Epub 2020 Mar 20.

872 Yu, J., Tostanoski, L.H., Peter, L., Mercado, N.B., McMahan, K., Mahrokhian, S.H., Nkolola, J.P.,
873 Liu, J., Li, Z., Chandrashekar, A., *et al.* (2020). DNA vaccine protection against SARS-CoV-2 in rhesus
874 macaques. Science. 2020 May 20;eabc6284. doi: 10.1126/science.abc6284. PMID: 32434945.

875 Yuan, M., Liu, H., Wu, N.C., Lee, C.D., Zhu, X., Zhao, F., Huang, D., Yu, W., Hua, Y., Tien, H., *et*
876 *al.* (2020). Structural basis of a shared antibody response to SARS-CoV-2. Science.

877 Zennou, V., Petit, C., Guetard, D., Nerhbass, U., Montagnier, L., and Charneau, P. (2000). HIV-1
878 genome nuclear import is mediated by a central DNA flap. Cell *101*, 173-185.

879 Zhao, J., Li, K., Wohlford-Lenane, C., Agnihothram, S.S., Fett, C., Zhao, J., Gale, M.J., Jr., Baric,
880 R.S., Enjuanes, L., Gallagher, T., *et al.* (2014). Rapid generation of a mouse model for Middle East
881 respiratory syndrome. Proc Natl Acad Sci U S A *111*, 4970-4975.

882 Zhu, F.C., Li, Y.H., Guan, X.H., Hou, L.H., Wang, W.J., Li, J.X., Wu, S.P., Wang, B.S., Wang, Z.,
883 Wang, L., *et al.* (2020). Safety, tolerability, and immunogenicity of a recombinant adenovirus type-5
884 vectored COVID-19 vaccine: a dose-escalation, open-label, non-randomised, first-in-human trial.
885 Lancet. 2020 Jun 13;395(10240):1845-1854. doi: 10.1016/S0140-6736(20)31208-3. Epub 2020 May
886 22. P.

Figure 1

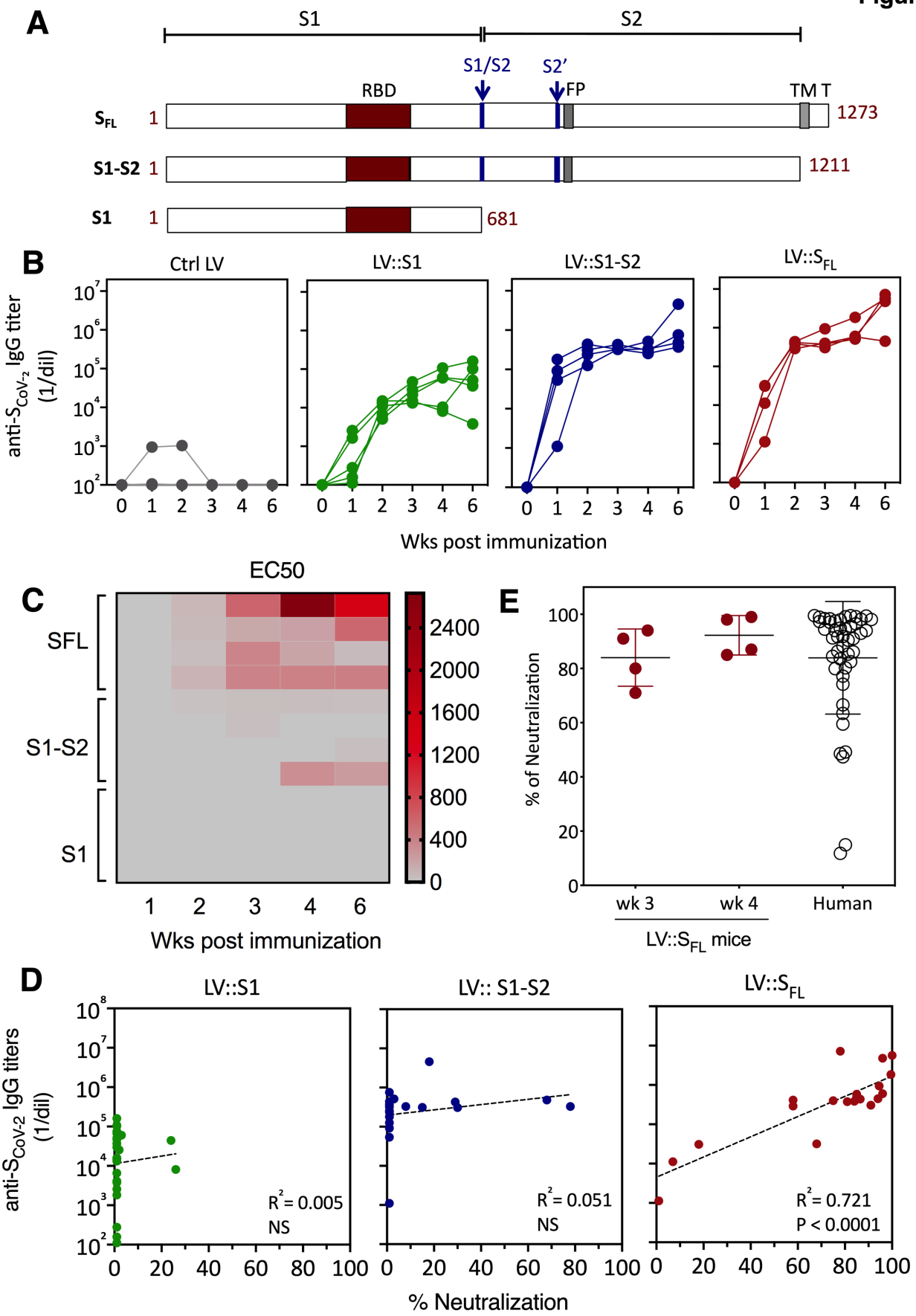
A
S1
S2
S1/S2
S2'
RBD
FP
TM T
S_FL
1
1273
S1-S2
1211
S1
681
B
Ctrl LV
LV::S1
LV::S1-S2
LV::S_FL
anti-S_CoV-2 IgG titer (1/dil)
Wks post immunization
C
EC50
SFL
S1-S2
S1
Wks post immunization
E
% of Neutralization
wk 3
wk 4
Human
LV::S_FL mice
D
LV::S1
LV:: S1-S2
LV::S_FL
anti-S_CoV-2 IgG titers (1/dil)
R² = 0.005
NS
R² = 0.051
NS
R² = 0.721
P < 0.0001
% Neutralization

887

Figure 2

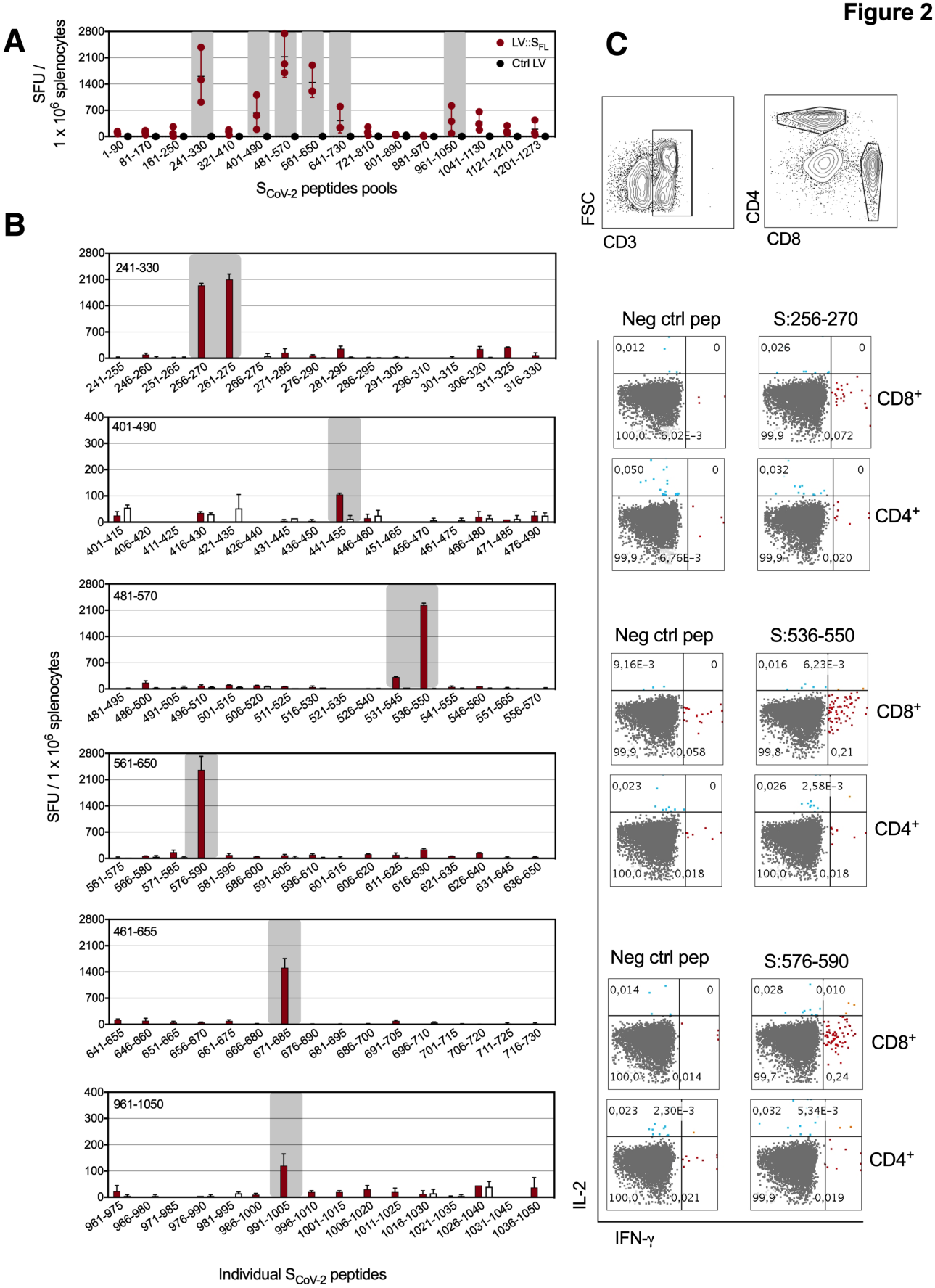
A
SFU / 1 x 10^6 splenocytes
LV::S_FL
Ctrl LV
S_CoV-2 peptides pools
B
241-330
401-490
481-570
561-650
461-655
961-1050
SFU / 1 x 10^6 splenocytes
Individual S_CoV-2 peptides
C
FSC
CD3
CD4
CD8
Neg ctrl pep
S:256-270
S:536-550
S:576-590
CD8+
CD4+
IL-2
IFN-γ

888

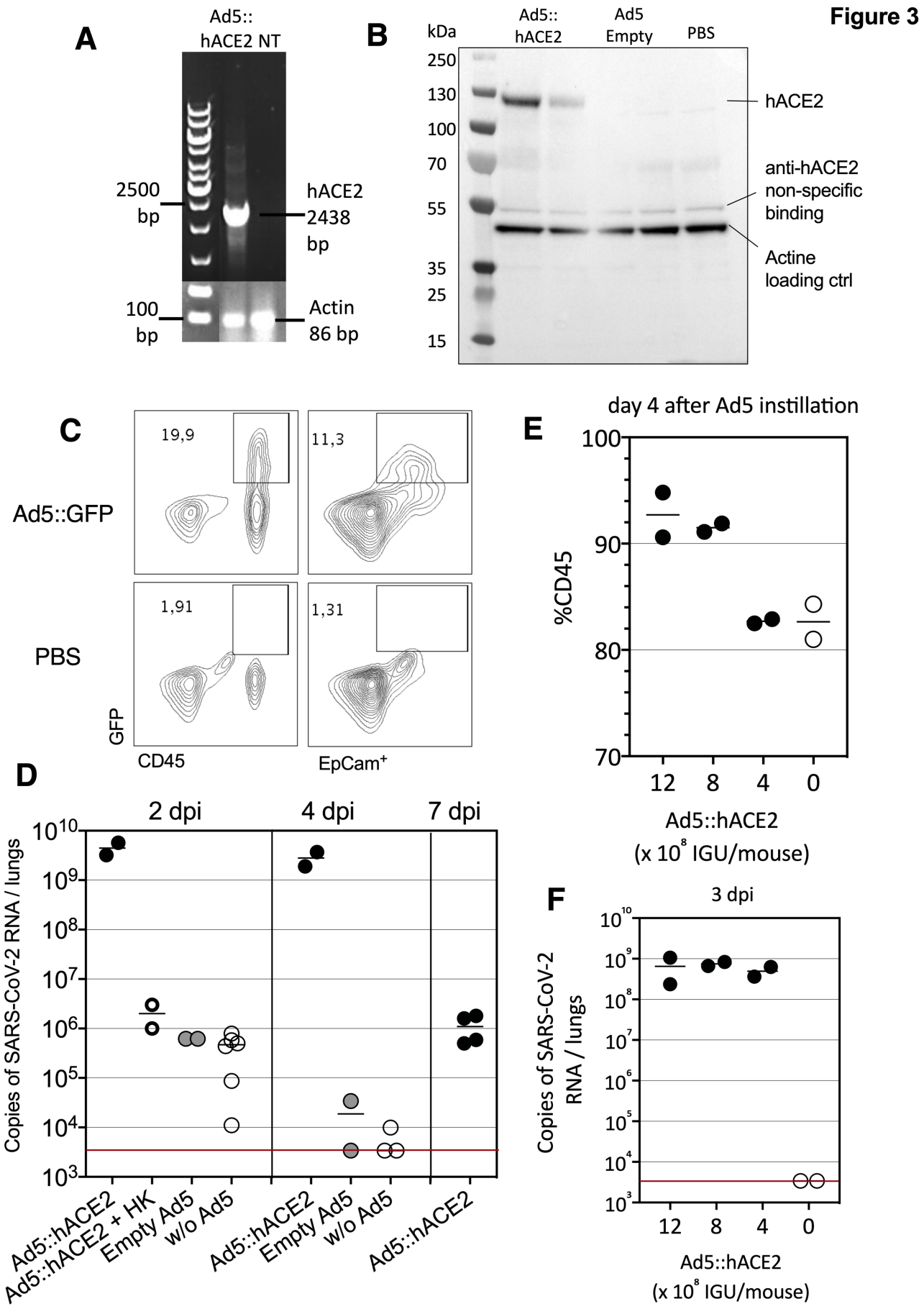
Figure 3
A
Ad5::
hACE2 NT
2500
bp
hACE2
2438
bp
100
bp
Actin
86 bp
B
kDa
Ad5::
hACE2
Ad5
Empty
PBS
250
130
100
70
55
35
25
15
hACE2
anti-hACE2
non-specific
binding
Actine
loading ctrl
C
Ad5::GFP
PBS
19,9
11,3
1,91
1,31
GFP
CD45
EpCam+
D
2 dpi
4 dpi
7 dpi
Copies of SARS-CoV-2 RNA / lungs
Ad5::hACE2
Ad5::hACE2 + HK
Empty Ad5
w/o Ad5
Ad5::hACE2
Empty Ad5
w/o Ad5
Ad5::hACE2
E
day 4 after Ad5 instillation
%CD45
Ad5::hACE2
(x 10^8 IGU/mouse)
F
3 dpi
Copies of SARS-CoV-2
RNA / lungs
Ad5::hACE2
(x 10^8 IGU/mouse)

889

Figure 4

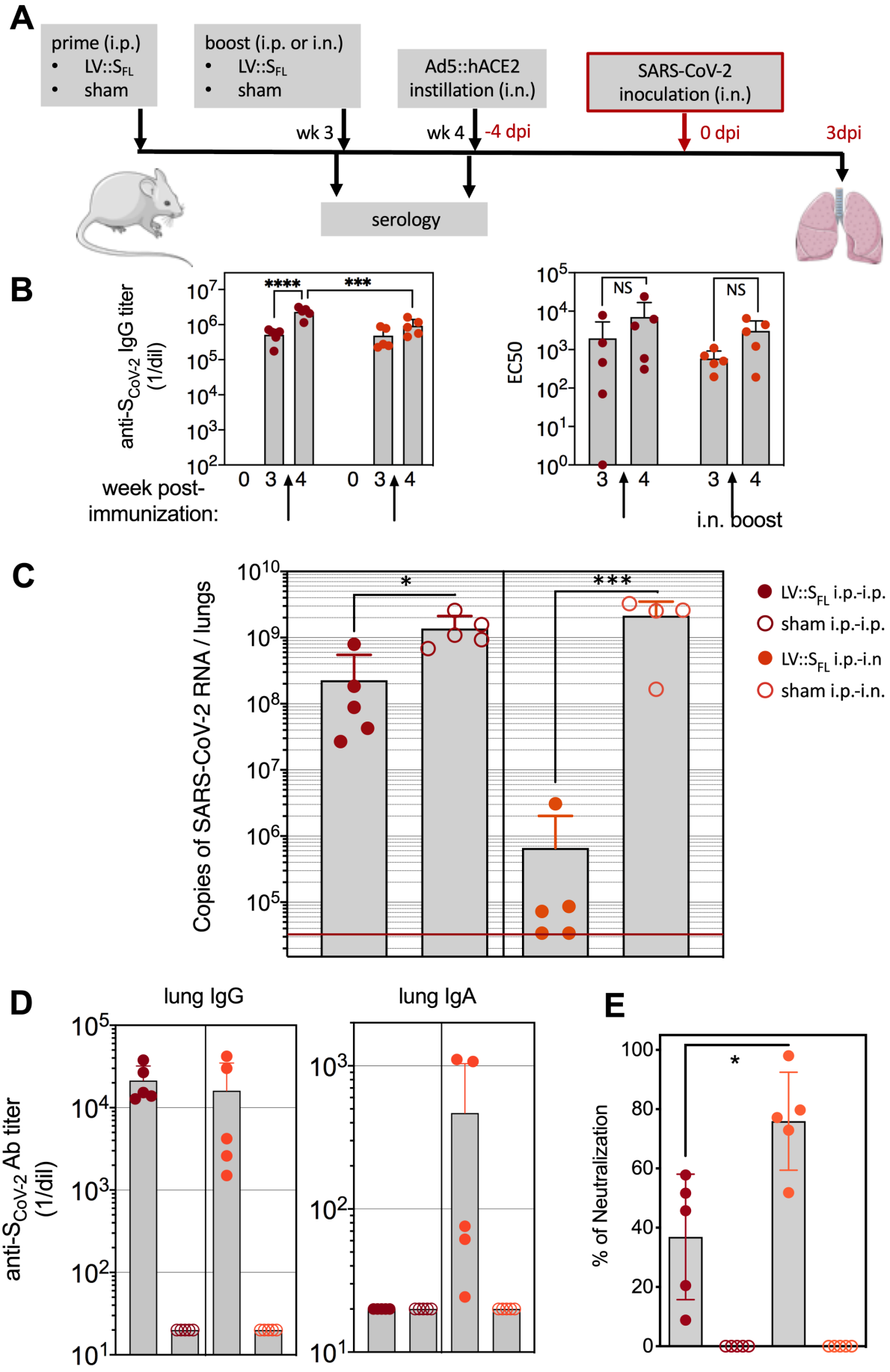
A
prime (i.p.)
• LV::S_FL
• sham
boost (i.p. or i.n.)
• LV::S_FL
• sham
Ad5::hACE2 instillation (i.n.)
SARS-CoV-2 inoculation (i.n.)
wk 3
wk 4
-4 dpi
0 dpi
3dpi
serology
B
anti-S_CoV-2 IgG titer (1/dil)
week post-immunization:
EC50
NS
i.n. boost
C
Copies of SARS-CoV-2 RNA / lungs
LV::S_FL i.p.-i.p.
sham i.p.-i.p.
LV::S_FL i.p.-i.n
sham i.p.-i.n.
D
lung IgG
lung IgA
anti-S_CoV-2 Ab titer (1/dil)
E
% of Neutralization

890

Figure 5

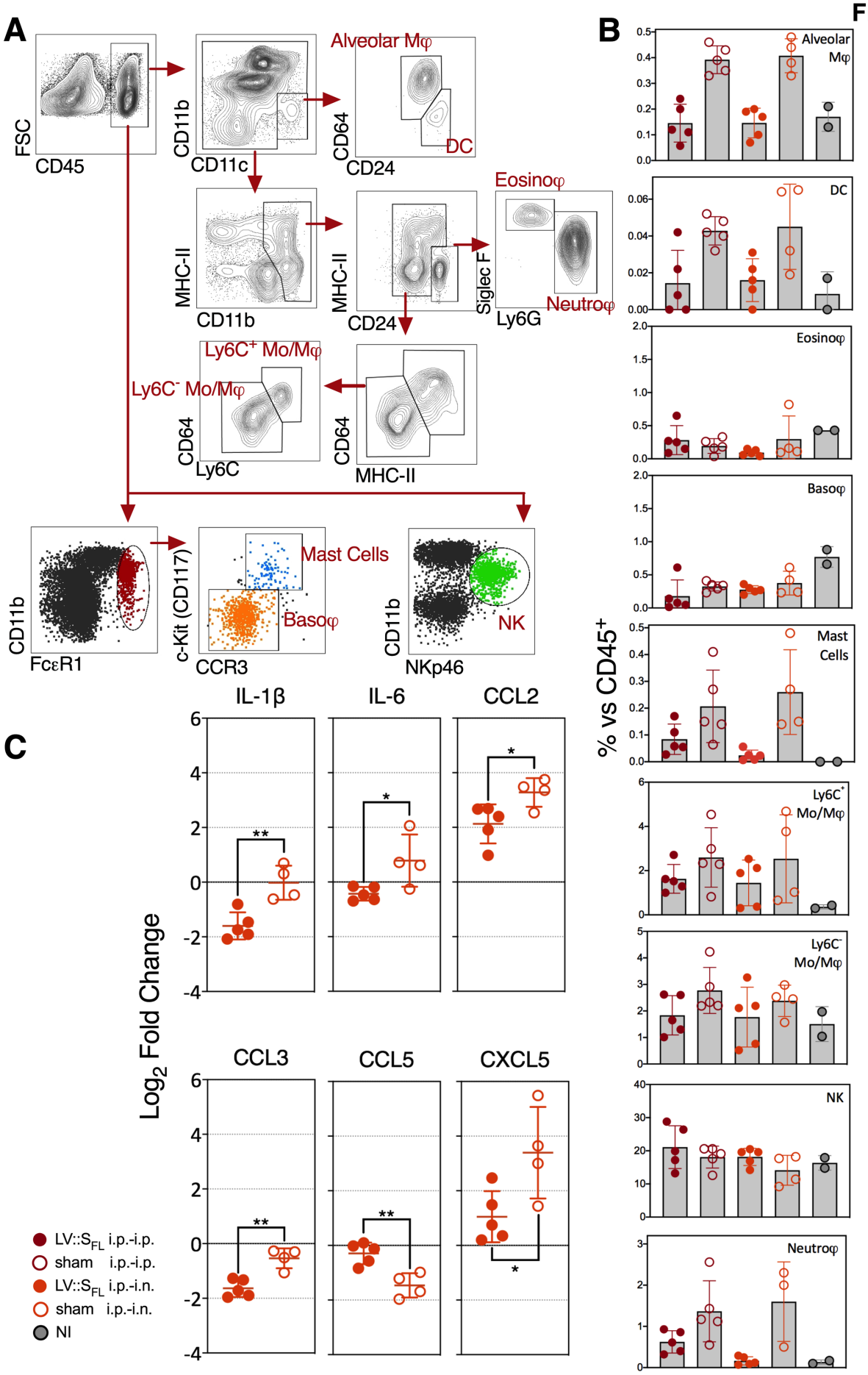
A
FSC
CD45
CD11b
CD11c
Alveolar Mφ
CD64
CD24
DC
MHC-II
CD11b
MHC-II
CD24
Siglec F
Ly6G
Eosinoφ
Neutroφ
Ly6C+ Mo/Mφ
Ly6C- Mo/Mφ
CD64
Ly6C
CD64
MHC-II
CD11b
FcεR1
c-Kit (CD117)
CCR3
Mast Cells
Basoφ
CD11b
NKp46
NK
B
% vs CD45+
Alveolar Mφ
DC
Eosinoφ
Basoφ
Mast Cells
Ly6C+ Mo/Mφ
Ly6C- Mo/Mφ
NK
Neutroφ
C
IL-1β
IL-6
CCL2
CCL3
CCL5
CXCL5
Log2 Fold Change
LV::SFL i.p.-i.p.
sham i.p.-i.p.
LV::SFL i.p.-i.n.
sham i.p.-i.n.
NI

891

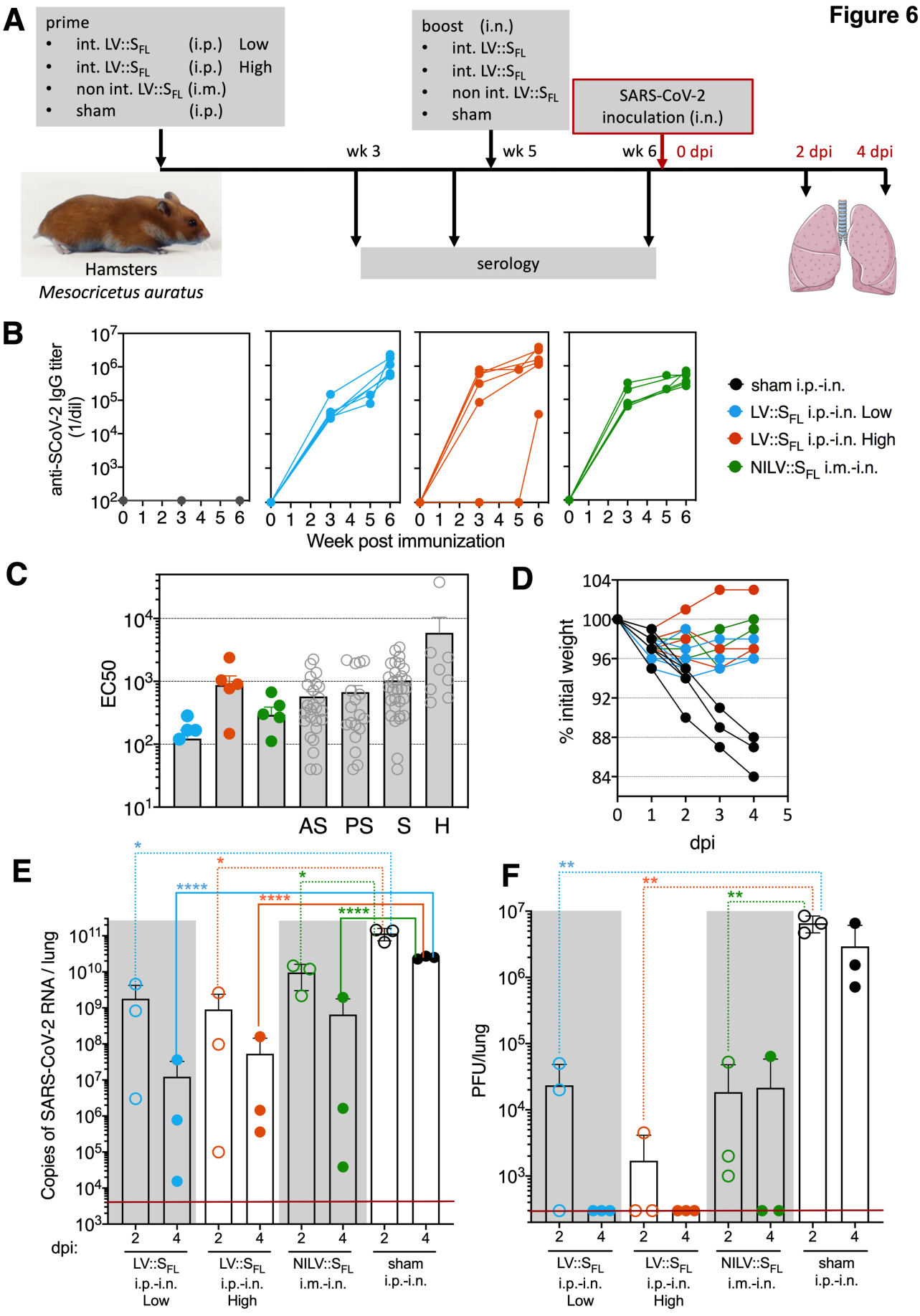
Figure 6
A
prime
int. LV::S_FL (i.p.) Low
int. LV::S_FL (i.p.) High
non int. LV::S_FL (i.m.)
sham (i.p.)
boost (i.n.)
int. LV::S_FL
int. LV::S_FL
non int. LV::S_FL
sham
SARS-CoV-2 inoculation (i.n.)
wk 3
wk 5
wk 6
0 dpi
2 dpi
4 dpi
Hamsters
Mesocricetus auratus
serology
B
anti-SCoV-2 IgG titer (1/dil)
Week post immunization
sham i.p.-i.n.
LV::S_FL i.p.-i.n. Low
LV::S_FL i.p.-i.n. High
NILV::S_FL i.m.-i.n.
C
EC50
AS
PS
S
H
D
% initial weight
dpi
E
Copies of SARS-CoV-2 RNA / lung
dpi:
LV::S_FL i.p.-i.n. Low
LV::S_FL i.p.-i.n. High
NILV::S_FL i.m.-i.n.
sham i.p.-i.n.
F
PFU/lung

892

Figure 7

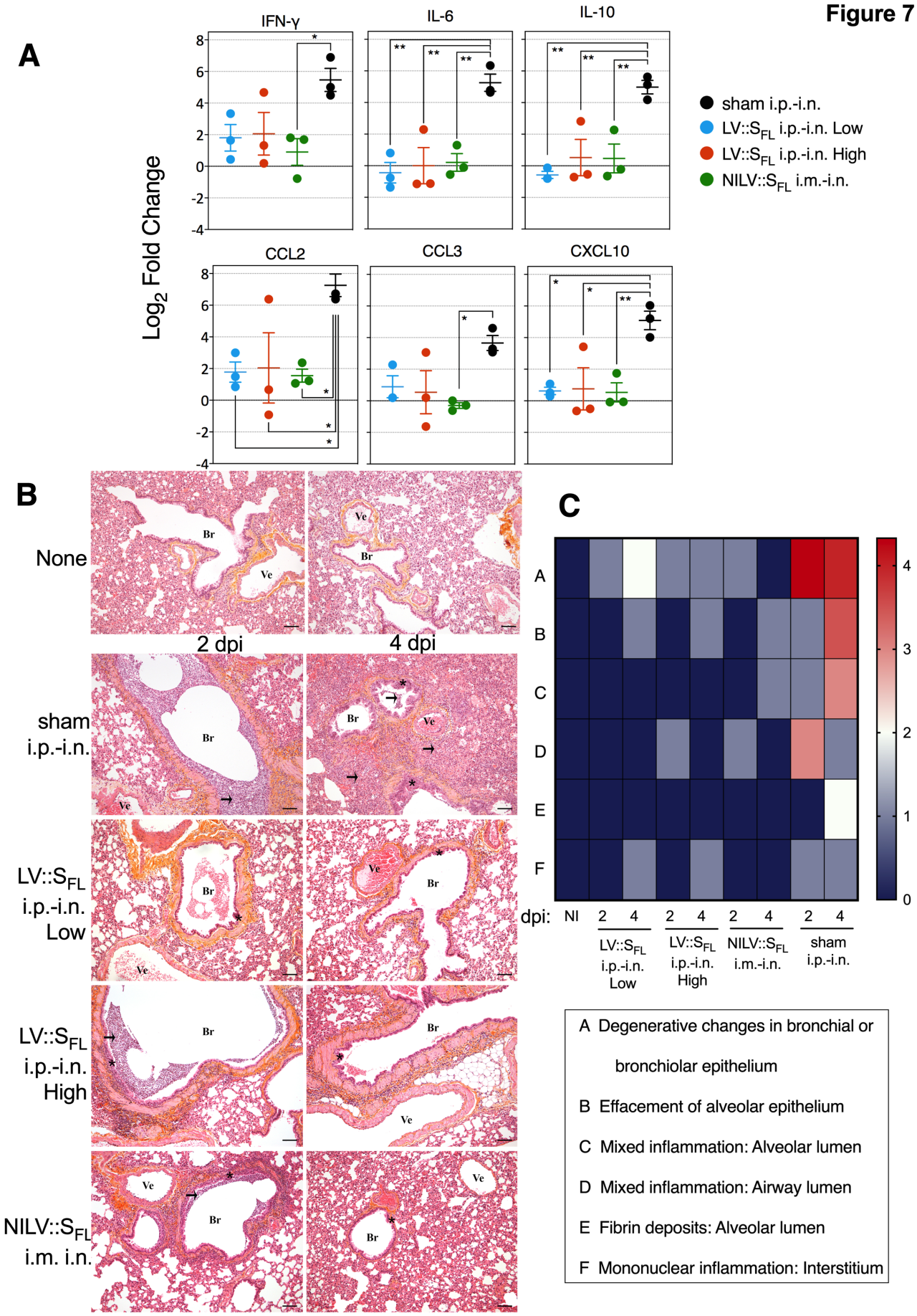
A
IFN-γ
IL-6
IL-10
CCL2
CCL3
CXCL10
Log2 Fold Change
sham i.p.-i.n.
LV::SFL i.p.-i.n. Low
LV::SFL i.p.-i.n. High
NILV::SFL i.m.-i.n.
B
None
2 dpi
4 dpi
sham i.p.-i.n.
LV::SFL i.p.-i.n. Low
LV::SFL i.p.-i.n. High
NILV::SFL i.m. i.n.
Br
Ve
C
A
B
C
D
E
F
dpi: NI 2 4 2 4 2 4 2 4
LV::SFL i.p.-i.n. Low
LV::SFL i.p.-i.n. High
NILV::SFL i.m.-i.n.
sham i.p.-i.n.
A Degenerative changes in bronchial or bronchiolar epithelium
B Effacement of alveolar epithelium
C Mixed inflammation: Alveolar lumen
D Mixed inflammation: Airway lumen
E Fibrin deposits: Alveolar lumen
F Mononuclear inflammation: Interstitium

893